



CHALMERS
UNIVERSITY OF TECHNOLOGY

Dynamics and stabilization mechanisms of amorphous solid dispersions

Master's thesis in Applied Physics

JOEL WANEMARK

MASTER'S THESIS 2016:06

**Dynamics and stabilization mechanisms of
amorphous solid dispersions**

JOEL WANEMARK



CHALMERS
UNIVERSITY OF TECHNOLOGY

Department of Physics
Condensed Matter Physics
CHALMERS UNIVERSITY OF TECHNOLOGY
Gothenburg, Sweden 2016

Dynamics and stabilization mechanisms of amorphous solid dispersions
JOEL WANEMARK

© JOEL WANEMARK, 2016.

Supervisor: Aleksandar Matic, Division of Condensed Matter Physics
Examiner: Aleksandar Matic, Division of Condensed Matter Physics

Master's Thesis 2016:06
Department of Physics
Division of Condensed Matter Physics
Chalmers University of Technology
SE-412 96 Gothenburg

Dynamics and stabilization mechanisms of amorphous solid dispersions
JOEL WANEMARK
Department of Physics
Chalmers University of Technology

Abstract

A growing problem in the pharmaceutical industry is the poor water-solubility of new candidate drugs^{22,41}. It is estimated that 75% of drugs under development are considered to have poor water-solubility¹⁹, and a low solubility heavily diminishes the chance of drug uptake and therapeutic effect. A method that has received attention lately to achieve increased solubility is to make use of a formulation strategy known as an amorphous solid dispersion (ASD)^{13,31}. The amorphous state of the pharmaceutical eliminates the impact of lattice energy resulting in increased solubility. However, since the pharmaceutical is in its thermodynamically metastable amorphous state, the dispersion may crystallize over relevant pharmaceutical timescales thus cancelling the solubility advantage. Stabilizing amorphous pharmaceuticals with polymers in ASDs have proven possible in previous studies^{5,42,63,59}, although the stabilization has been attributed to different mechanisms.

In this work, the relationship between anti-plasticization effects and hydrogen bonding was investigated in ASDs with ibuprofen and felodipine using dielectric spectroscopy, differential scanning calorimetry and FTIR spectroscopy. The physical stability of ibuprofen was drastically improved, stabilizing the drug in its amorphous state over a timescale of months. It was found that the polymeric glass transition temperature of the polymer did not correlate with the stabilization effect of ibuprofen. The effect was instead attributed to hydrogen bonding between polymer and ibuprofen. Dispersions using felodipine were however not successfully prepared.

Keywords: ibuprofen, solid dispersion, relaxation dynamics, stabilization, crystallization.

Acknowledgements

First of all, I would like to acknowledge and gratefully thank my supervisor and examiner professor Aleksandar Matic. His guidance and scientific expertise along with his endless support and motivational attitude have all been crucial to this thesis. I would also like to give special thanks to my colleagues at the division of Condensed Matter Physics at Chalmers University of Technology. They have provided me with not only helpful scientific advice and discussions but also a lot of laughter and a fantastic work environment.

Joel Wanemark, Gothenburg, 06 2016

Contents

1	Introduction	1
2	Aim	3
3	Theory	5
3.1	The Amorphous State	5
3.1.1	Glass transition	5
3.1.2	Characterization of the amorphous state	7
3.2	Crystallization	8
3.3	Amorphous Solid Dispersion	9
3.3.1	Two-component mixing	9
3.3.2	Glass transition in ASDs	11
3.4	Characterization Methods of Amorphous Solid Dispersions	12
3.4.1	Differential scanning calorimetry	12
3.4.2	Broadband dielectric spectroscopy	14
3.4.2.1	Analysis of dielectric spectra	15
3.4.3	Analyzing crystallization kinetics	17
4	Materials	21
4.1	Felodipine	21
4.2	Ibuprofen	22
4.3	HPMCAS	23
4.4	PVP	23
4.5	Soluplus®	24
5	Methods	25
5.1	Solvent casting	25
5.2	Differential Scanning Calorimetry	26
5.3	Dielectric Spectroscopy	26
6	Results & Discussion	27
6.1	Single Component Dynamics	27
6.1.1	Relaxation dynamics of felodipine	28
6.1.2	Relaxation dynamics of ibuprofen	30
6.1.3	Relaxation dynamics of HPMCAS	30
6.1.4	Relaxation dynamics of PVP K30	32
6.1.5	Relaxation dynamics of Soluplus®	33

6.2	Solid Dispersion Dynamics	34
6.2.1	Ibuprofen : HPMCAS	35
6.2.2	Ibuprofen : PVP	37
6.2.3	Ibuprofen : Soluplus®	41
6.2.4	Comparison of dynamics in dispersions	44
6.3	Crystallization Inhibition of Solid Dispersions	47
6.4	Stabilization Mechanisms	51
7	Conclusion	55
7.1	Summary	55
7.2	Outlook	55
	Bibliography	57
A	Supporting Information	I
A.1	DSC thermograms	I
A.2	Raman Analysis	III
A.3	Crystallization Kinetics	IV

1

Introduction

A growing problem in the pharmaceutical industry is the high hydrophobicity and poor water-solubility of new drug candidates^{41,22}. This has the effect that the bioavailability, which is a measure on how much of the drug that reaches the systematic circulation, drops drastically. Estimations are that approximately 40% of currently marketed drugs and 75% of drugs under development are considered to have poor water-solubility¹⁹. The reasons behind this trend are multiple and increased potency desires and exploration of unprecedented drug targets are just two of many reasons⁶⁶. For some applications the poor water-solubility can be circumvented by liquid formulations but for oral drug administration, which is the most frequently used drug formulation method⁶, the market demands traditional solid dosage forms⁶⁶.

The greatest concern with high hydrophobicity and poor water-solubility in oral administration is the risk of reduced and variable absorption of the drug in the body. Upon release, the pharmaceutical must first dissolve into the gastric fluid and then molecularly be absorbed by the gastrointestinal system in order to enter the bloodstream and subsequently its intended target. Hence, a low solubility heavily diminishes the chance of drug uptake and therapeutic effect. Important to note though is that the value at which the limited solubility starts to impact absorption is difficult to determine since it is dependent on a number of variables. One way to increase the drug uptake is to increase the dosage, but limited water-solubility creates difficulties in predicting the absorbed drug concentration and the concentration could therefore reach toxic levels.

The risk of too low or too high drug concentration is not the only drawback of the poorly water soluble drugs, the release and uptake profile is also a major hindrance. To keep the dosage frequency as low as possible a release profile that is as extended as possible with a constant drug release is preferable. For poorly water soluble drugs though, the release profile varies and is difficult to predict. One method that has received attention lately to achieve both increased solubility and controlled release is to make use of a formulation strategy known as an amorphous solid dispersion (ASD)^{13,31}. An amorphous solid dispersion consists of an active pharmaceutical ingredient (API) that is amorphous within a carrier matrix which usually is polymeric, although other materials have also been investigated^{26,65}. The amorphous state exhibits a disordered structure and stabilizing the pharmaceutical in its amorphous state instead of in its crystalline state as in regular formulations eliminates the impact of lattice energy resulting in increased solubility. Further-

more, a polymeric additive could be able to sustain high concentration of the API within the gastric fluid thus creating an extended release profile.

However, since the pharmaceutical is in a thermodynamically metastable amorphous state, the dispersion can be unstable over relevant pharmaceutical timescales and the API may crystallize thus cancelling the solubility advantage. Therefore various ways of stabilizing amorphous pharmaceuticals with polymers have been put forward in literature. The stabilization has been attributed to different mechanisms, including for example anti-plasticization by the polymer⁶³, interactions between the API and the polymer^{59,46}, a reduction in local molecular mobility⁵, and an increase in the activation energy of nucleation⁴². The role of the different mechanisms are illustrated in figure 1.1.

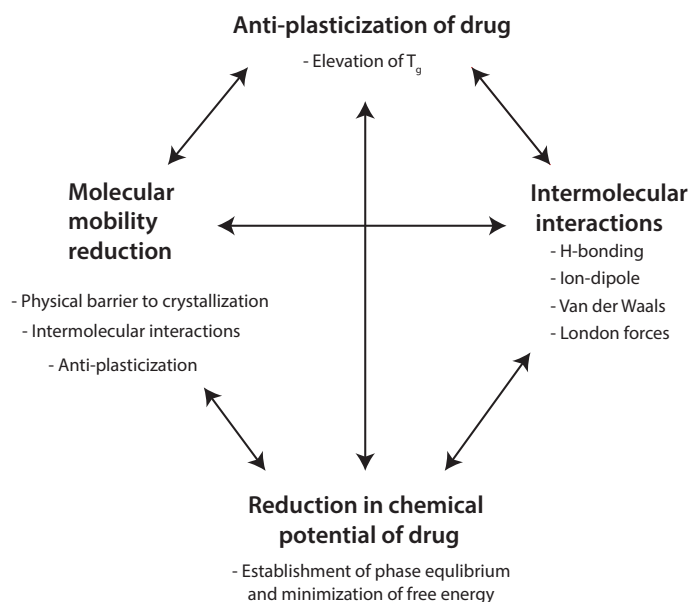


Figure 1.1: Overview of the different mechanisms that could be responsible for stabilizing a drug in its amorphous state. The focus in this thesis will be on the interplay between anti-plasticization and intermolecular interactions.

Despite extensive research the mutual relations between these processes are not fully understood and polymer selection is still largely empirical⁹. The present knowledge is concentrated to specific drug-polymer combinations, and this thesis therefore seeks to do a broader comparison. Two different pharmaceuticals are investigated, felodipine and ibuprofen, and three different polymers are used as carrier matrices. The polymer selection (HPMCAS, PVP K30, Soluplus®) was based on previously reported glass transition temperatures of the polymers (160°C, 120°C, 70°C respectively), and their different abilities to form hydrogen bonds. This way, the relationship between anti-plasticization effects and hydrogen bonding is investigated.

2

Aim

The aim of this thesis is to investigate the dynamics of polymeric amorphous solid dispersions and the stabilization mechanisms of amorphous pharmaceuticals using polymers as carrier matrices. This will be done by:

- characterizing the properties and dynamics of the two pharmaceuticals and three polymers of interest.
- analyzing the dynamics of the pharmaceutical components when confined in the polymers.
- studying the change of polymer dynamics when adding the pharmaceuticals.
- studying the hydrogen bonding interactions between the pharmaceuticals and polymers.
- monitoring the crystallization process for the neat APIs and dispersions and comparing kinetic parameters.

2. Aim

3

Theory

In the following sections, the theoretical background of physical concepts discussed in this thesis is given as well as a description of measurement and analysis methods.

3.1 The Amorphous State

The amorphous state is differentiated from the crystalline state by the lack of long range translational order with repeating units and patterns. Amorphous solid materials has been known for a long time but it was not until the latest century that the term lost its equivalence with the term glasses. Nowadays glasses are a subset of the amorphous solids and the importance of amorphous materials is increasing with applications in for example optical fibers and pharmaceuticals. However, a theoretical framework modeling the solid amorphous material dynamics is not present to date.²¹

3.1.1 Glass transition

For a material to become a glass it must be cooled through the glass transition without crystallizing. Crystallization occurs when a liquid is cooled at a rate where the atoms or molecules have sufficient time to move around and lock in to their respective minimum in the energy landscape. This creates a discontinuity in both volume, entropy and enthalpy as a function of temperature, as can be seen in figure 3.1, which is characteristic for a first-order phase transition.

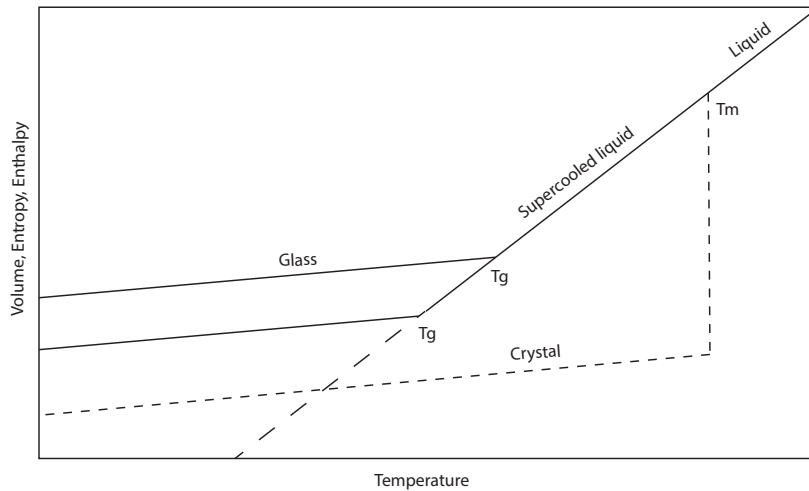


Figure 3.1: *Schematic behavior of volume, entropy and enthalpy versus temperature. If the liquid crystallizes, a step-like change can be seen at the melting temperature T_m . If the liquid is cooled at a high enough rate, the liquid enters the supercooled region and then reaches a temperature T_g which denotes the glass transition. The two different T_g marked in the figure denotes the glass transition temperature for different cooling rates.*

However, if the liquid is cooled fast enough the crystallization can be avoided and the liquid then enters what is called the supercooled region as marked in figure 3.1. The lowered kinetic energy of the atoms or molecules hinders them from moving to an energy minimum and creates a metastable state with respect to the crystalline state. If the liquid then is cooled further the viscosity increases drastically and the liquid freezes into an amorphous solid without any ordered structure at a temperature which is denoted as the glass transition temperature, or T_g as marked in figure 3.1. The viscosity at the glass transition is 10^{12} Pa s and despite its name, the glass transition is not a true thermodynamical phase transition since it is cooling rate dependent. The slower the liquid is quenched the lower the glass transition temperature will be as displayed by the two different glass transition temperatures in figure 3.1, but it is of importance that the liquid is cooled fast enough to avoid recrystallization. At the glass transition temperature, the relaxation time τ that determines the time-scale of molecular displacements and reorientations crosses the experimental timescale and becomes 100-1000 s²¹. Therefore molecular motions virtually cease and the system falls out of equilibrium. The molecular displacement relaxation is usually denoted as the α -relaxation, and other relaxations relating to intramolecular motions as for example polymer side group reorientations are called secondary relaxations. Important to note is that below T_g there might still be secondary relaxations present, although the α -relaxation ceases.

3.1.2 Characterization of the amorphous state

To characterize the supercooled liquid and the glassy state, several measures are used. First off, in general neither the α -relaxation time nor the viscosity η follow an Arrhenius temperature dependence, i.e. $\tau \propto \exp(\Delta E/k_b T)$. This causes a deviation from the Arrhenius line in the Angell plot, as shown in figure 3.2¹².

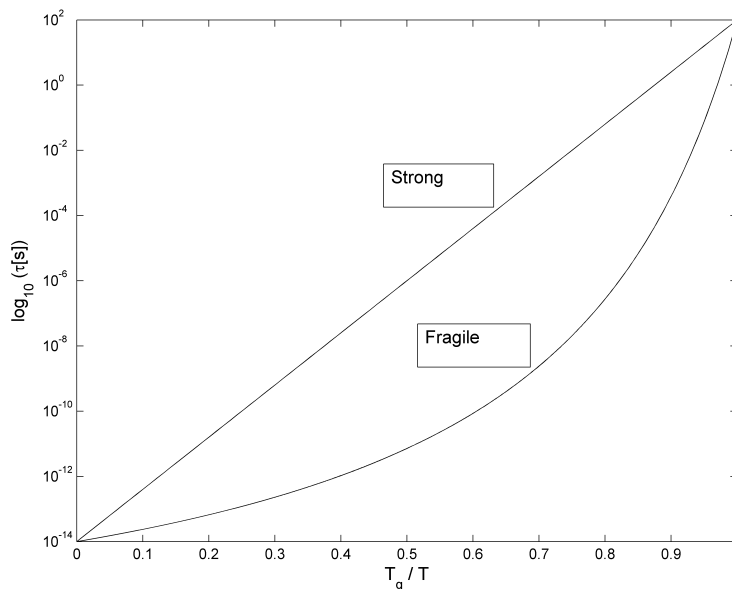


Figure 3.2: Schematic of relaxation time τ as a function of T_g/T . Strong liquids display linear Arrhenius behavior while fragile liquids deviate from the linearity.

Instead, most liquids have a relaxation time temperature dependence that follows the Vogel-Fulcher-Tammann equation

$$\tau = \tau_0 \exp\left(\frac{DT_0}{T - T_0}\right) \quad (3.1)$$

where $\tau_0 \sim 10^{-13}$ s, which is a typical microscopic time. The parameter D is used to distinguish between liquids close to Arrhenius behavior that have a high D value, so called strong liquids, and fragile liquids that have low D values⁴⁹ as shown in figure 3.2. Another measure is the so-called fragility index m which is defined¹⁰ as

$$m = \left. \frac{d(\log_{10} \tau_\alpha(T))}{d\left(\frac{T_g}{T}\right)} \right|_{T=T_g} \quad (3.2)$$

where a higher value ($m > 80$) implies a more fragile liquid. Fragile materials have structures that change rapidly with temperature around T_g , and thermal excitations are able to cause structural reorganizations over a variety of particle orientations and coordination states. As these reorganizations might induce crystallization, the fragility parameter m may be a parameter that can help to predict the ease of crystallization^{4,68}.

3.2 Crystallization

It is of great importance that the API remains in the amorphous state to achieve the desired bioavailability increase, and it is therefore crucial to understand and analyze mechanisms that can cause it to crystallize. If an amorphous solid is kept in the supercooled region, it is metastable with respect to the crystalline state and can therefore crystallize. The crystallization occurs through a process called nucleation, in which a critical number of molecules self-assemble into the stable state and form a nucleus from which crystallization is then extended. However, both the nucleation probability and the subsequent crystal growth rate is highly dependent on the studied material and the experiment conditions⁴. When discussing nucleation and crystallization it is important to separate between the two different nucleation processes known as homogeneous and heterogeneous nucleation. Homogeneous nucleation is caused by thermal fluctuations that overcome the energy barrier needed to create a spherical nucleus. The energy barrier consists of the energy gain by forming the crystal nucleus and the energy cost of forming a liquid-solid interface and is given by the free energy equation³⁴

$$\Delta G(r) = \frac{4\pi r^3}{3} \Delta G_b + 4\pi r^2 \gamma \quad (3.3)$$

where ΔG_b is the change in free energy on going from liquid to solid, γ is the interface energy, and r is the nucleus radius. This free energy has a maximum value for a critical nucleus size r^* where nuclei smaller than this size are unstable and nuclei larger than the size are less probable. At this size the free energy is given by

$$\Delta G(r^*) = \frac{16\pi\gamma^3}{3\Delta G_b^2} \quad (3.4)$$

Thus, a thermal fluctuation with energy surpassing this energy barrier can create a stable nucleus and once that has happened, subsequent crystal growth is energetically favorable. This energy barrier can however be greatly reduced by the presence of dirt particles, a container wall, or something else that can act as a nucleation site, and then it is called heterogeneous nucleation. This type of nucleation is therefore far more common in experiments than homogeneous nucleation because of the difficulty in avoiding impurities³⁴. This however can lead to slower crystallization growth rates as the number of nucleation sites is limited and there could be a so-called nucleation site saturation, whereas homogenous nucleation is not bound to specific sites. Furthermore, even though heterogeneous nucleation might be energetically favorable the process might not take place. The thermodynamic driving force is increased with lowered temperature but as the temperature approaches T_g there is a dramatic increase in viscosity thus introducing a kinetic element to nucleation. Since molecules need to move to nucleate, the increased viscosity might inhibit the crystallization. Characterization of crystallization is explained in detail in section 3.4.3.

3.3 Amorphous Solid Dispersion

To be able to make use of the enhanced solubility of amorphous APIs crystallization has to be prevented. This can be done by using an additive (or carrier) to stabilize the amorphous state creating an amorphous solid dispersion (ASD). Ever since the introduction of the term in the early 1960's⁵⁵, different preparation methods and stabilization additives have been developed, and different types can be distinguished depending on the state of carrier and API. First off all the carrier matrix can be either crystalline or amorphous, but since the carrier matrices in this thesis are polymers that are amorphous, crystalline matrices will not be discussed. Within the amorphous carrier matrix the API can be sustained in three different states; i) as crystalline particles, ii) as amorphous particles or iii) molecularly dispersed, as illustrated in figure 3.3. To be able to achieve the desired amorphous state of the API, it is crucial to understand the underlying theory of solid dispersions and the following sections therefore give an overview of the relevant theoretical framework.

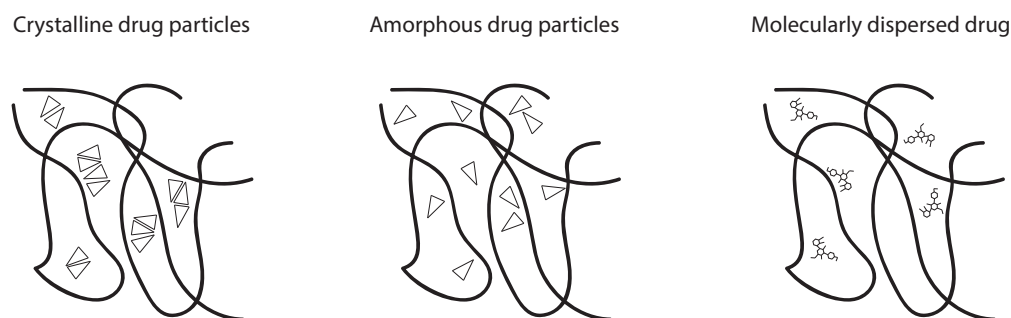


Figure 3.3: Illustration of the three different states of the pharmaceutical ingredient within the polymer matrix; i) crystalline form, ii) in amorphous clusters, or iii) molecularly dispersed.

3.3.1 Two-component mixing

Even in the amorphous state of dispersion, shown as state ii and iii in figure 3.3, local concentration differences might occur. Higher local concentrations of the amorphous drug increase the risk of crystallization, and thus the homogeneity of mixing is important⁶⁴. When mixing the API and polymer the miscibility is dependent on the interaction energies within and between the individual components, and the free energy of mixing

$$\Delta G_{mix} = \Delta H_{mix} - T\Delta S_{mix} \quad (3.5)$$

needs to be negative. An model of this free energy term is called the Flory-Huggins equation and is defined as

$$\Delta G_{mix} = RT [n_1 \ln(\phi_1) + n_2 \ln(\phi_2) + n_1\phi_2\chi_{12}] \quad (3.6)$$

where n_1, n_2 denote the respective number of moles, ϕ_1, ϕ_2 the respective volume fractions and χ is the interaction parameter between the components. The first two terms represents entropic contributions and since mixing leads to entropy increase

3. Theory

these terms almost always favor mixing. The third term is the enthalpy contribution, and it is governed by the interaction parameter $\chi \propto T^{-1}$. Thus, a large value on χ , or low temperatures, promotes immiscibility of the system. Furthermore, the miscibility also depends on the drug-polymer ratio as displayed in figure 3.4.

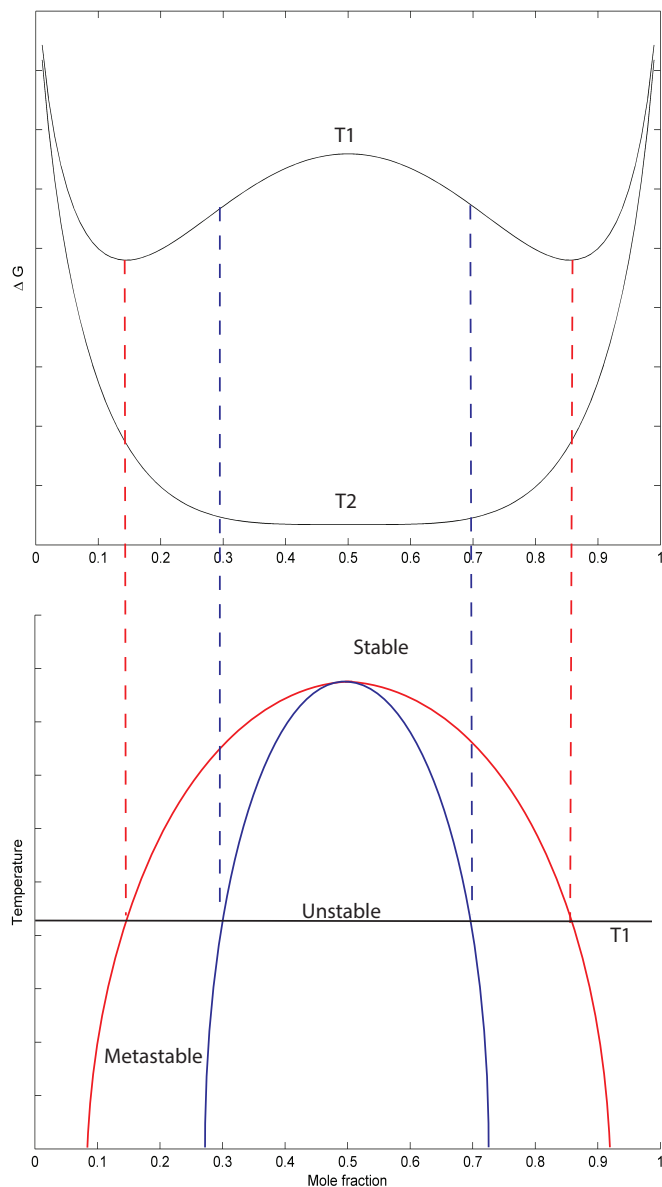


Figure 3.4: *Top: free energy vs mole fraction for two different hypothetical temperatures. The two minima of free-energy are marked with dashed red lines and the inflection points, where the second derivative is zero, are marked with blue dashed lines. Bottom: the phase boundary is marked with a solid red line and the spinodal line is shown with a solid blue line. These separate the stable, metastable and unstable regions. The temperature T1 is marked with a black line.*

In figure 3.4, the free energy vs mole fraction is shown for two different temperatures and the translation of these into so-called binodal and spinodal locus curves. At a

fixed temperature miscibility is limited by the free-energy minimum as shown with dashed red lines in the figure. Plotting the free energy minimum for a range of temperatures creates a phase boundary line as illustrated with a solid red line in the figure. Outside this line the liquid is miscible and stable. Inside this line, i.e. within the immiscible region, two phases exist that phase-separate using different mechanisms, and the line separating them are found by looking at the second derivative of the free-energy, as illustrated in figure 3.4 as dashed and solid blue lines. The compositions in between the two distinct regions are metastable to relatively small molecular fluctuations, and phase separation by nucleation occurs as described in section 3.2. In the case of ASDs, this way of phase separation is usually hindered by the limited mobility and therefore the limited energy available to form a nucleus of critical size. Inside the unstable region phase separation occurs continuously through diffusion of molecules which is called spinodal decomposition, and is thus closely linked to the α -relaxation. This increase in local drug concentration gives rise to an increased risk of crystallization as stated before⁶⁶. Thus it is of importance to either have a dispersion with a large stability window or to efficiently inhibit the recrystallization within the metastable and unstable states. As with most theories, their applicability to actual systems are limited and experiments have shown both to follow the predictions of the Flory-Huggins and contradict it⁵³. Nevertheless it can give a prediction of the miscibility of the drug-polymer system.

3.3.2 Glass transition in ASDs

The increased complexity by mixing two components also transfers into the prediction of what happens to the system's relaxation behavior. When discussing the glass transition earlier in section 3.1.1 only a single component was considered. When adding a second component complexity is added to the system. To this date numerous methods to predict the T_g of a mixture have been developed. The most widely used is the Gordon-Taylor equation²⁸

$$T_{g,mix} = \frac{w_1 T_{g,1} + K w_2 T_{g,2}}{w_1 + K w_2} \quad (3.7)$$

where w_1, w_2 are the respective weight fractions, $T_{g,1}, T_{g,2}$ the respective glass transition temperatures and the constant K is dependent on the densities ρ and thermal expansivities $\Delta\alpha$ and defined as

$$K = \frac{\rho_1 \Delta\alpha_1}{\rho_2 \Delta\alpha_2}. \quad (3.8)$$

Thus blending the API with a polymer with a higher T_g results in a system T_g that should fall somewhere in between the individual T_g s. The Gordon-Taylor equation was derived using two critical assumptions; the ideal volume additivity of both components at T_g , and that there are no specific interactions between the components i.e. ideal mixing behavior. Hence, the equation only holds when the components are fully miscible over the entire composition regime. In a similar approach developed by Couchman-Karaz¹⁴ the constant K is defined as

$$K = \frac{\Delta C_{p,2}}{\Delta C_{p,1}} \quad (3.9)$$

where ΔC is the respective specific heat capacities at their T_g s. No model to date can fully predict the behavior of the glass transition of solid dispersions. It is important to note a couple of things: i) a single T_g is not necessarily a sign of homogeneity of the ASD, although multiple T_g s is significant for an immiscible mixture⁵⁴ and ii) there is no definitive correlation between the T_g and the physical stability of the ASD although a higher T_g in general increases the stability of an ASD⁸. The difficulties in predicting the behavior can be explained both by experimental difficulties as well as difficulties in predicting component interactions⁸. Experimental difficulties are dominated by the influence of moisture which usually has a large plasticizing effect, i.e. increasing molecular mobility and lowering the T_g . Drug-polymer interactions can be both ion-dipole interactions as well as intermolecular H-bonding between drug and polymer, and their role is not easily predicted. A study of ASDs with ketoconazole (KTZ) showed a strong ionic interaction with poly(acrylic acid) (PAA) and weaker dipole-dipole interactions with PVP, and it showed that dispersions with PAA elevated the T_g of the API more than dispersions with PVP⁴⁵. In another system, nifedipine (NIF) formed hydrogen bonds with both PVP and PAA and the ability to elevate the API T_g was reversed³⁷. Therefore understanding the intermolecular interactions is crucial in analyzing the glass transition in ASDs.

3.4 Characterization Methods of Amorphous Solid Dispersions

To study the phase behavior, i.e. glass formation and crystallization, and structural relaxation processes within the ASDs two methods are used in this thesis, Differential Scanning Calorimetry (DSC) and Dielectric Spectroscopy (DS). In the following sections the theory behind the methods is explained and their advantages and limitations are discussed. The experimental set-ups are described in section 5, where also secondary characterization methods are introduced and briefly explained.

3.4.1 Differential scanning calorimetry

Differential Scanning Calorimetry (DSC) is a thermal analysis technique that is widely used to study phase transitions such as melting, crystallization and glass transitions. Using a small sample (\sim mg) and an empty reference pan, the heat flow difference between the sample and the empty reference is measured as a function of temperature. Since the DSC works at constant pressure, the heat flow is equivalent to the enthalpy change. In endothermic processes the sample heat flow will be higher than the reference's and will therefore show as a negative heat flow and the opposite for exothermic processes. The result of a DSC measurement is called a thermogram and is schematically depicted in figure 3.5, where the characteristics signatures of different thermal processes are shown.²³

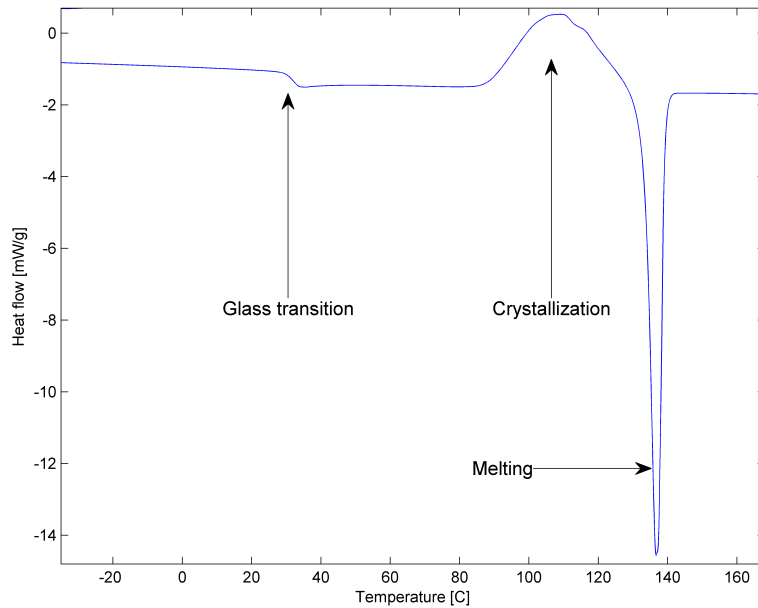


Figure 3.5: Schematic DSC thermogram showing heat flow versus temperature. Characteristics of glass transitions, crystallization and melting are indicated.

In this thesis, the glass transition is of interest. To determine the glass transition temperature three different measures can be used; either onset, endset or midpoint as shown in figure 3.6. The midpoint is usually defined as the maximum of the first derivative of heat flow, and this measure will be used throughout this thesis when discussing DSC T_g ²³.

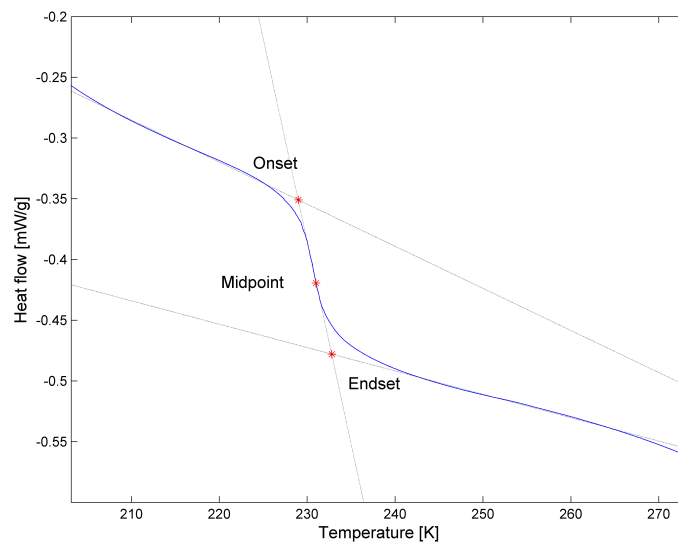


Figure 3.6: DSC thermogram showing heat flow versus temperature and the different methods of calculating T_g . Onset, midpoint and endset are shown. Throughout this thesis the midpoint method is used.

The main advantage of DSC is easy sample preparation and relatively short running time. One major drawback is the difficulty to analyze thermograms of compounds with overlapping thermal events, especially when it comes to the often small heat flow change at the glass transition. One way to circumvent this is to use Modulated DSC (MDSC) which instead of a linear increase of temperature uses two simultaneous heating rates - one linear and one sinusoidal. The sinusoidal heating rate enables the separation of the heat flow signal into reversing and non-reversing components through Fourier transform deconvolution.⁶⁰ The reversible heat flow reveals heat capacity changes such as a glass transition, while the non-reversible heat flow signal reveals kinetic events such as crystallization. By doing this, a higher resolution around the glass transition is achieved thus resulting in more accurate results⁶⁰. A drawback of the DSC is the inability to analyze the underlying dynamics governing the transitions, thus other characterization methods are needed.

3.4.2 Broadband dielectric spectroscopy

Dielectric spectroscopy is an excellent method to study the dynamics of liquids and glasses. The method is based on the interaction between the electric dipole moment of the sample and an applied external field. Depending on the molecular structure and dynamics of the sample the dipole moment responsive motions are different and one can accordingly draw conclusions of the sample dynamics. Note that in the following description of the theoretical background for dielectric spectroscopy the material will be considered to be isotropic, which is a valid assumption in an ASD.

When applying an electric field over the material, the material is polarized. At not too strong electric fields, the polarization field \vec{P} is defined as

$$\vec{P} = (\varepsilon - 1)\varepsilon_0\vec{E} \quad (3.10)$$

where ε is the frequency dependent complex dielectric function and ε_0 is the vacuum permittivity. This expression is then used in the electric displacement field \vec{D} definition

$$\vec{D} = \varepsilon_0\vec{E} + \vec{P} = \varepsilon\varepsilon_0\vec{E}. \quad (3.11)$$

When applying a periodic disturbance $E(\omega, t) = E_0 \exp(-i\omega t)$, the resulting displacement field is then expressed as $D(t) = D_0 \exp(-i(\omega t + \phi(\omega)))$ and the dielectric properties of the material determine the amplitude D_0 and the phase shift $\phi(\omega)$. Using these field expressions we get that

$$\varepsilon^*(\omega) = \varepsilon'(\omega) - i\varepsilon''(\omega) = \frac{D(\omega)}{\varepsilon_0 E} = \frac{D_0}{\varepsilon_0 E_0} \exp(-i\phi(\omega)). \quad (3.12)$$

The complex and imaginary parts of the complex dielectric function are then related through the Kramer-Kronig relations,

$$\varepsilon'(\omega) = 1 + \frac{2}{\pi} P \int_0^\infty \frac{\nu \varepsilon''(\nu)}{\nu^2 - \omega^2} d\nu \quad (3.13)$$

$$\varepsilon''(\omega) = \frac{2\omega}{\pi} P \int_0^\infty \frac{\varepsilon'(\nu) - 1}{\nu^2 - \omega^2} d\nu$$

3.4.2.1 Analysis of dielectric spectra

In dielectric spectroscopy, the complex dielectric function $\varepsilon(\omega)$ is measured over a range of frequencies. A conceptual illustration of the dielectric spectrum is shown in figure 3.7. In the figure, a liquid is held at constant temperature $T > T_g$ and the figure shows the real and imaginary parts of the dielectric function ε^* . The specific features in the spectrum are related to different processes within the material. A peak in the imaginary part ε'' and a step-like decrease of the real part ε' are both a sign of a relaxation process. An increase of ε'' with a slope -1 with decreasing frequency is related to conduction phenomena. Conduction arises from charge transport and the conductivity contribution is highly dependent on the number of mobile charge carriers and temperature. For pure ohmic conduction ε' is frequency independent while for non-ohmic conduction or polarization effects ε' increases with decreasing frequency, as noted in figure 3.7.

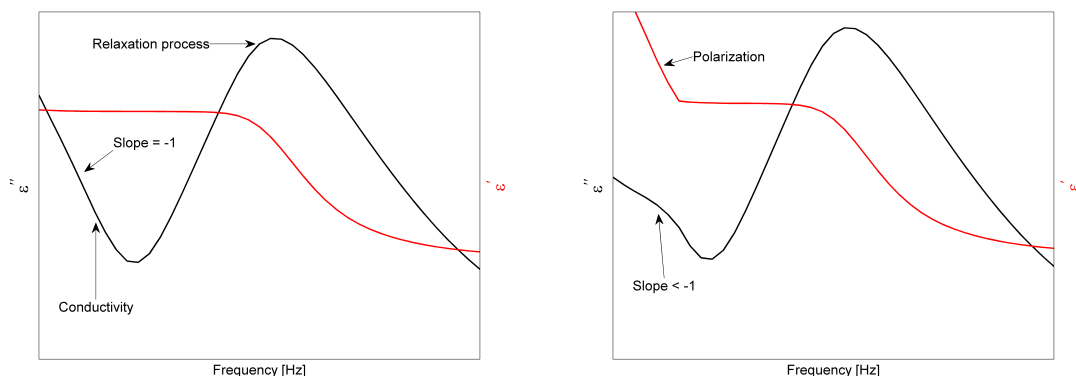


Figure 3.7: *Conceptual illustration of a dielectric spectrum displaying both the real part (red) and the imaginary part (black). The left figure shows pure ohmic conduction for low frequencies that has a slope of -1 in the imaginary part and is frequency independent in the real part. The right figure also displays electrode polarization that distorts the low frequency part of both spectra.*

The different relaxation processes are usually divided into either α -relaxations, β -relaxations or other secondary relaxations. The α -relaxation corresponds in the API to molecular displacements and in polymers to segmental motions of polymer chains. The secondary relaxations typically have either intra- or intermolecular origin, and are denoted differently. The Johari Goldstein-relaxation, which is thought to be a universal feature of all glass formers²⁹, corresponds to local reorientation of entire molecules and could therefore be a precursor for the molecular mobility. Other β -processes are usually intramolecular and are usually denoted β, γ, δ etc with decreasing timescale. By analyzing the dielectric function, information about the dynamics can be obtained. Peaks in the imaginary part of the dielectric function at a certain frequency f_p relate to characteristic relaxation times $t_p = 1/2\pi f_p$, and by studying how these relaxation times change with temperature one is able to draw conclusion on the liquid dynamics. For an ideal, noninteracting population of dipoles subjected to an external alternating field the response is described by the

Debye-relaxation¹⁸ equation

$$\varepsilon^*(\omega) = \varepsilon_\infty + \frac{\Delta\varepsilon}{1 + i\omega\tau_D} \quad (3.14)$$

where ε_∞ is the permittivity at the high frequency limit, $\Delta\varepsilon = \varepsilon_S - \varepsilon_\infty$ where ε_S is the permittivity at the low frequency limit, and τ_D is the characteristic relaxation time. However, for non-ideal relaxations other model functions are used. In this thesis a model function called the Havriliak-Negami function is used. It is a modification of the Debye equation and is defined³³ as

$$\varepsilon^*(\omega) = \varepsilon_\infty + \frac{\Delta\varepsilon}{(1 + (i\omega\tau_{HN})^{\alpha_{HN}})^{\beta_{HN}}} \quad (3.15)$$

where α_{HN} and β_{HN} define the shape of the peak and $0 < \alpha, \beta \leq 1$. The parameter β_{HN} describes an asymmetric broadening of the relaxation function for frequencies $f_{HN} > 1/\tau_{HN}$, while α_{HN} describes a symmetrical broadening. Special cases of the equation occur and one is the so-called Cole-Davidson case where $\alpha_{HN} = 1$. This function is usually used to fit the α -relaxation as it typically exhibits asymmetric broadening. The parameter β_{HN} then affects the relaxation function as shown in figure 3.8. Important to note is that the characteristic relaxation time of the model function does not coincide with the relaxation time related to the maximal loss.

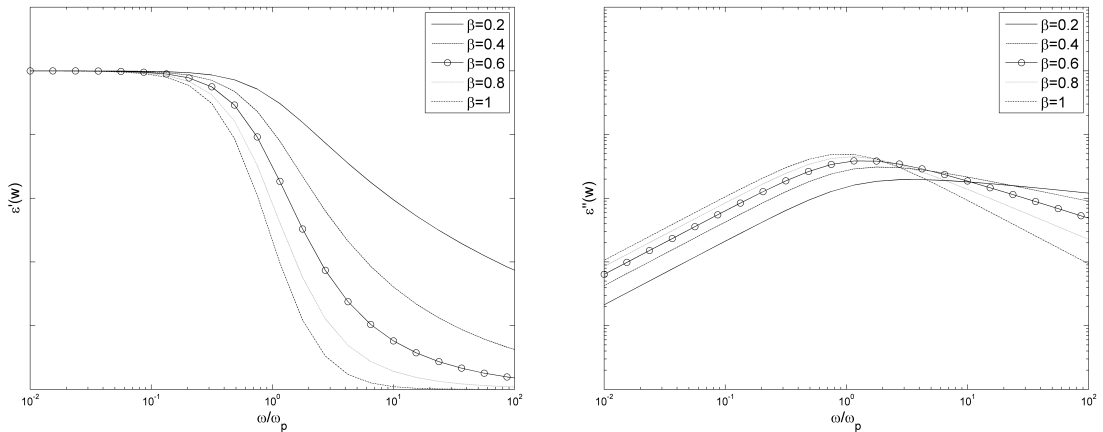


Figure 3.8: *Effect of the asymmetric broadening parameter β_{HN} of the Havriliak-Negami function in the Cole-Davidson case where $\alpha_{HN} = 1$.*

Another special case is the Cole-Cole function where instead $\beta_{HN} = 1$. It is commonly used to fit β -relaxation processes. How α_{HN} effects the shape of the Cole-Cole relaxation function is shown in figure 3.9.

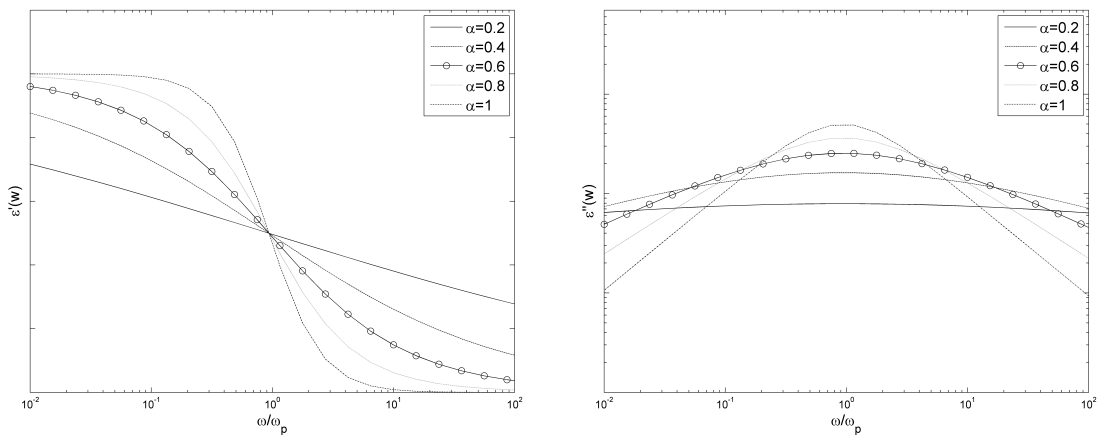


Figure 3.9: *Effect of the symmetric broadening parameter α_{HN} of the Havriliak-Negami fitting function in the Cole-Cole case where $\beta_{HN} = 1$.*

As experimental data are analyzed isolated relaxation processes are rarely found. Instead several relaxation processes and conductivity contributes to the spectrum. The conductivity contribution is accounted for as

$$\varepsilon = \varepsilon_{HN} - i \frac{\sigma_0}{\varepsilon_0 \omega^s} \quad (3.16)$$

where the parameter s is set to 1 if there is no polarization of the electrodes. If the different relaxations are independent, which in most cases is a valid assumption, the complex dielectric functions are additive and then the fitting procedure uses least square minimizing

$$\sum_i w_i \left[\varepsilon_i^* - \left(\sum_k \varepsilon_{HN,k}^*(\omega_i) - i \frac{\sigma_0}{\varepsilon_0 \omega_j^s} \right) \right]^2 \rightarrow \min \quad (3.17)$$

where i counts the experimental data points, k is the number of HN-functions, and w is a weighting factor to correct for data accuracy differences. The fitting can be carried out using either the imaginary or the real part of ε'' , and literature show that they give nearly identical results³⁸.

3.4.3 Analyzing crystallization kinetics

To be able to analyze and evaluate the crystallization kinetics of a liquid, the sample needs to be monitored during the crystallization process. In this thesis, dielectric spectroscopy has been used. However the method adds surfaces that could increase the risk for heterogeneous nucleation. Since the strength of the dielectric signal is proportional to the number of fluctuating dipoles in the sample, as crystallization occurs a smaller volume fraction of the sample fluctuates and the strength of the signal decreases⁴⁸. This decrease can then be monitored as a function of time at constant temperature to analyze the crystallization kinetics. At a specific frequency, chosen often as the loss peak frequency of the α -relaxation, the recorded signal can

3. Theory

be converted to a degree of crystallinity X through^{16,43}

$$X(t) \propto \varepsilon_N(t) = \frac{\varepsilon''(t_0) - \varepsilon''(t)}{\varepsilon''(t_0) - \varepsilon''(\infty)} \quad (3.18)$$

where t_0 is the crystallization onset time and ε_N is the normalized dielectric strength. This normalized dielectric function then follows⁴⁸ an exponential decay as

$$X(t) = 1 - \exp\left(-\left(\frac{t - t_0}{\tau_c}\right)^n\right) \quad (3.19)$$

where X is the degree of crystallinity, τ_c is the characteristic timescale of crystallization and t_0 is the induction time for crystallization. The parameter n is correlated to the time dependence of the nucleation rate and indicates an heterogenous or homogenous character of the nucleation, the dimensionality of the process⁴⁸, and information about the dimensions of the growing crystal¹⁵. This approach however assumes that the density of the crystal and the liquid is the same, that the nucleus does not move in the remaining melt, and that the direction of growth is linear with respect to the radial distance from the nucleus center⁴⁸.

By determining τ_c and n using either the Avrami method or the Avramov method, conclusions can be drawn on crystallization kinetics. The Avrami method, developed in the 1940's, is based on taking the double logarithm of the normalized function and plotting it versus the logarithm of t and analyzing the linear regime, as exemplified in figure 3.10.

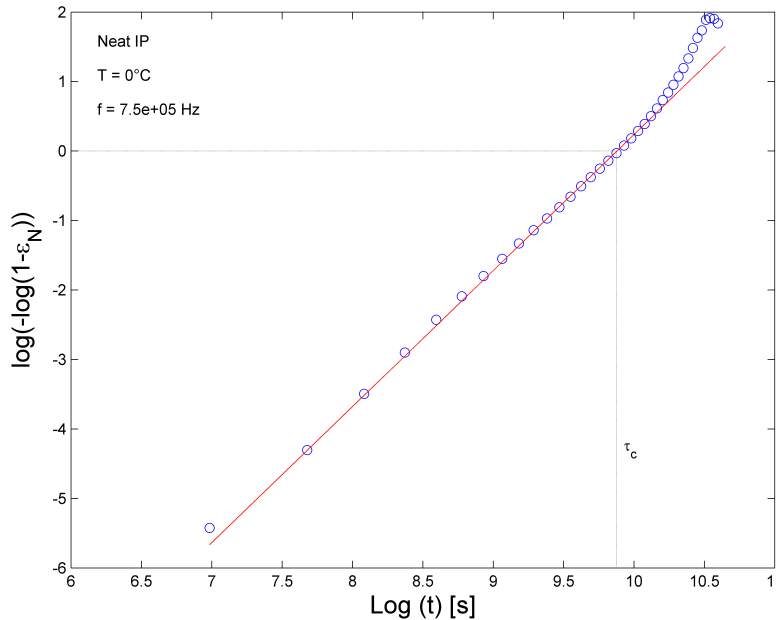


Figure 3.10: Avrami plot of neat ibuprofen kept at 0 °C.

From the slope of the line the value of n can be estimated and by studying where the line crosses $y = 0$, i.e. when $\varepsilon_N = 1 - e^{-1}$, it is possible to determine τ_c . In

this way it is possible to estimate the induction time t_0 through $\tau_c = t - t_0$, but it can not be obtained directly. Furthermore, several studies have shown difficulties in obtaining a straight line, especially at high/low ε_N values, thus decreasing the accuracy of the method^{1,48}.

To overcome the drawbacks of the Avrami method, Avramov developed a method⁷ using the derivative of the normalized dielectric function, as exemplified in figure 3.11. The peak in the derivative is used to estimate τ_c , and the parameter n is estimated as

$$n = \frac{(\varepsilon_n)'_{max}}{1/e} \quad (3.20)$$

where $(\varepsilon_n)'_{max}$ is the maximum of the first derivative of the normalized dielectric function.

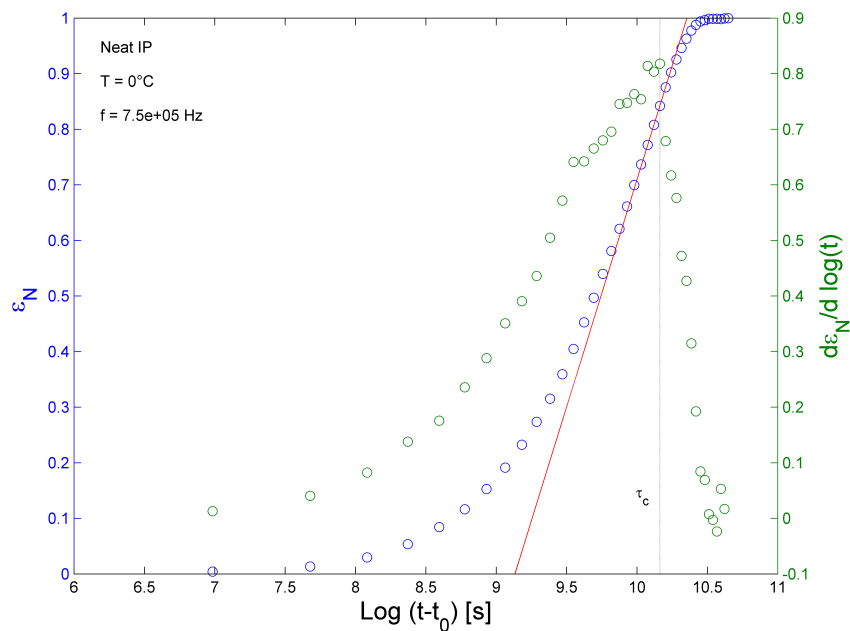


Figure 3.11: Avrami plot of neat ibuprofen kept at 0 °C.

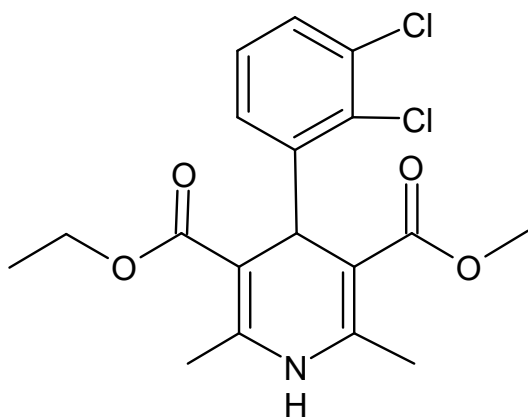
4

Materials

The following section presents the chemical structure and chemical data of the drugs and polymers used in this thesis. The active pharmaceutical ingredients Felodipine and Ibuprofen were selected based on extensive literature references and availability. The polymers were selected based on their different glass transition temperatures and abilities to form hydrogen bonds.

4.1 Felodipine

Felodipine is a dihydropyridine calcium antagonist used to control hypertension (high blood pressure) and it was supplied by Astra Zeneca. Due to its low solubility it has been the focus of many studies on solubility enhancement using ASDs^{62,67}. The chemical structure is shown in figure 4.1 along with material properties.

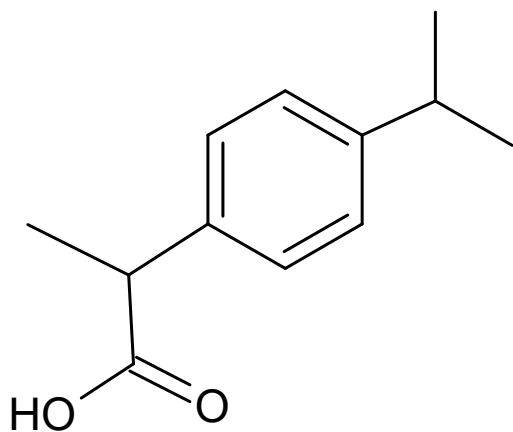


Chemical formula	$C_{18}H_{19}NO_4$
CAS-number	72509-75-3
Molecular weight	384.25 g/mol
T_m	142°C ⁶⁷
T_g	46°C ⁴²

Figure 4.1: Chemical structure, physical and chemical data of felodipine.

4.2 Ibuprofen

Ibuprofen is a pharmaceutical compound used worldwide because of its analgesic, antipyretic and antiinflammatory properties²⁷. In this thesis Ibuprofen from Sigma Aldrich was used. The chemical structure of Ibuprofen (2-[4-(2-methylpropyl)phenyl]propanoic acid) is shown in figure 4.2 along with chemical data as well as physical properties .



Chemical formula	$C_{13}H_{18}O_2$
CAS-number	15687-27-1
Molecular weight	206.28 g/mol
T_m	$77^{\circ}C^1$
T_g	$-45^{\circ}C^{20,11}$

Figure 4.2: *Chemical structure, physical and chemical data of ibuprofen.*

4.3 HPMCAS

Hydroxypropyl methyl cellulose acetate succinate (HPMCAS) is a polymer widely used in literature to study the stabilization of ASDs and has been proven to effectively prevent re-crystallization of the API³⁶. In this work Affinisol™ HPMC-AS 716 G (Dow Pharma & Food) was used, and the chemical structure is shown in figure 4.3.

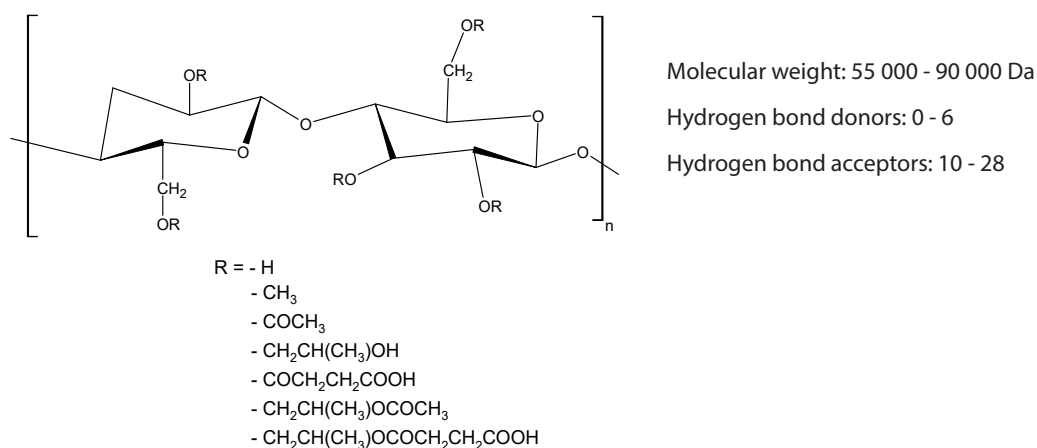


Figure 4.3: Chemical structure and chemical data of HPMCAS.

4.4 PVP

Poly(vinylpyrrolidone), or PVP, has just as HPMCAS been widely studied and has been proven to stabilize drugs in their amorphous state in ASDs⁹. PVP is available in many different grades of polymerization characterized by the K-value, and in this thesis PVP K30 was used (Povidone K 29-32, Sigma Aldrich). The chemical structure and ability to form hydrogen bonds are shown in figure 4.4.

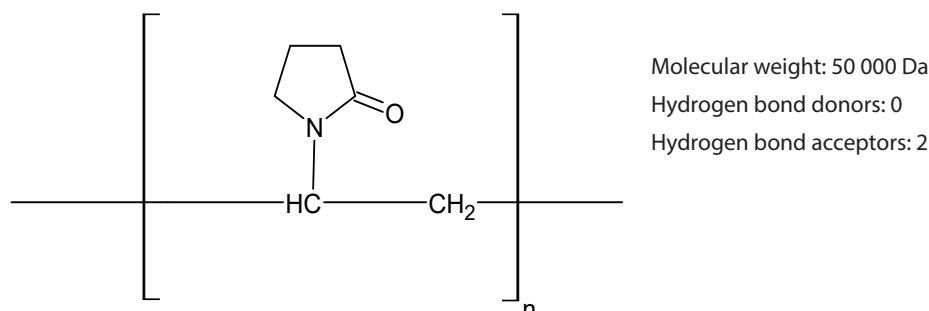


Figure 4.4: Chemical structure and chemical data of PVP.

4.5 Soluplus®

Soluplus® (SOL) is a graft copolymer composed of polyethylene glycol, polyvinyl caprolactam and polyvinyl acetate introduced by BASF. The foremost advantage of Soluplus® is its low glass transition temperature, thus having an ability to be used in the hot melt extrusion preparation method together with drugs that degrade at high temperatures. For the purpose of this thesis, Soluplus® was chosen because of its low glass transition temperature (70°C^{32}). The chemical structure and the relevant data of Soluplus® are shown in figure 4.5.

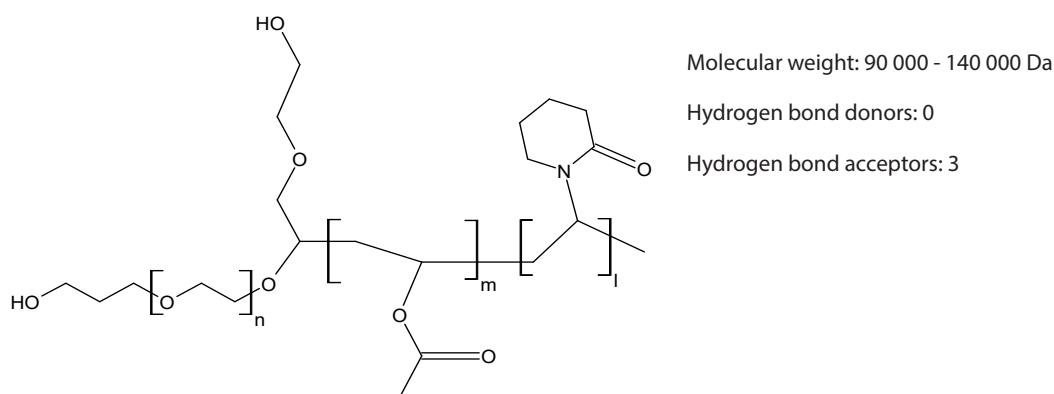


Figure 4.5: Chemical structure and chemical data of Soluplus®.

5

Methods

The following sections describe the solvent casting method used to prepare the amorphous solid dispersions. Additionally the methods used for characterizing both neat pharmaceuticals and polymers as well as the amorphous solid dispersions are described in detail. The following procedures were followed throughout the thesis work unless otherwise noted.

5.1 Solvent casting

Multiple methods to prepare amorphous solid dispersions have been reported throughout literature and solvent casting is one of them⁶⁶. The decision to use solvent casting was based on the availability and simple procedure of the method. Nevertheless, the method had to be modified to fit each type of polymer:API combination as previously reported methods did not suit all combinations.

The pharmaceutical ingredient and polymer of choice were dissolved in a 1:1 solvent mixture of dichloromethane and ethanol. The API:polymer w/w ratio was varied and so was also the components:solvent w/v ratio to find an appropriate amount of solvent (around 2-5% w/v). The solution was stirred for several hours until complete dissolution of the polymer, determined by visual inspection, and then casted onto an appropriate mold. The dispersions were covered with pieces of parafilm with holes to slow down evaporation and then left to evaporate for at least 12 hours in a fume hood, and finally dried in a vacuum oven at 60°C for at least 12 hours. The samples were weighed pre-evaporation, post-evaporation and post-annealing to ensure complete solvent evaporation.

Early DSC measurements of PVP:IP20 dispersions displayed differences in glass transition temperature and they were therefore analyzed using Raman spectroscopy. The difference was concluded to come from different polymer concentrations within the sample and not from remaining solvent, see details in section A.2, thus confirming a successful evaporation.

For DSC measurements most of the dispersions were casted onto a petri dish. For some dispersions with high polymer concentration problems with the subsequent extraction occurred. These were instead casted onto a 5 micron PTFE film glued to the bottom of a weighing boat. For dielectric measurements the dispersions were casted directly onto the stainless steel electrodes using a teflon mold.

5.2 Differential Scanning Calorimetry

Differential Scanning Calorimetry, DSC, experiments were carried out using a TA instruments Q1000. The samples were prepared and weighed in air and at room temperature and then sealed hermetically in an aluminum pan by a TA Tzero press. Helium and nitrogen were used as purge gases, flow ratee 25 ml/min. In the standard DSC measurements, a heating rate of 10 K/min was applied. For the modulated DSC measurements a modulation amplitude of 1.3 K and a modulation period of 60 s were used, based on litterature references⁶¹.

5.3 Dielectric Spectroscopy

Dielectric spectra of the substances and the dispersions were measured using a Novo-control Dielectric Spectrometer. The measuring system was equipped with a Quatro Cryosystem (-160°C - 400°C), an Alpha analyzer (10^{-2} - 10^7 Hz), and a standard sample cell BDS 1200. Measurement control was carried out by WinDeta software and data analysis was made with WinFit software and MATLAB. The temperature range for each expperiment was determined case by case based on hypotheses by the author and limited by thermal degradation temperatures of the sample components. All measurements were performed in with the frequency range 10^{-2} - 10^7 Hz.

6

Results & Discussion

The following sections present the physical properties and dynamics of the components of interest. First of all the individual components are analyzed and thereafter the results for the solid dispersions are presented. Lastly, the crystallization kinetics in both the neat states and in the dispersions are investigated.

6.1 Single Component Dynamics

To be able to properly evaluate the characteristics of the solid dispersions, thorough analyses of the single components were needed and the results are shown in the following sections. The single components were characterized using mainly DSC and dielectric spectroscopy, and a summary of the results from the DSC measurements are shown in table 6.1. Previous results found in literature are also shown in the table and a strong agreement is found. The DSC thermograms are found in supporting information A.1.

Table 6.1: Summary of the glass transition and melting temperatures for all components determined in this work (left columns) and literature reference values (right columns).

Component	T_g [°C]		T_m^* [°C]	
Felodipine	43 ± 2	$46^{8,42}$	150 ± 2	$145^{8,42}$
Ibuprofen	-43 ± 1	$-45^{1,8}$	77 ± 2	$76^{1,8}$
HPMCAS	$114 \pm 6^\diamond$	119^{51}	-	N/A
PVP K30	$165 \pm 5^\diamond$	$160-177^{25,47}$	-	$\sim 180^{52\dagger}$
Soluplus®	60 ± 1	$\sim 70^{32,44}$	~ 140	N/A

* T_m for polymers defined as the temperature where the polymer have liquid-like behavior.

† Most studies show no such behavior.^{25,56}

◇ Polymer showed large variations in T_g .

6.1.1 Relaxation dynamics of felodipine

An example of the imaginary part of the dielectric spectrum from neat felodipine is shown in figure 6.1, together with an example of a fit with two HN functions and a conductivity term. To the right, spectra are shown for three different temperatures and one can then clearly see how the relaxation process shifts towards higher frequencies as temperature is increased. The shift towards faster relaxation times is expected since a temperature increase leads to increased mobility of the molecules.

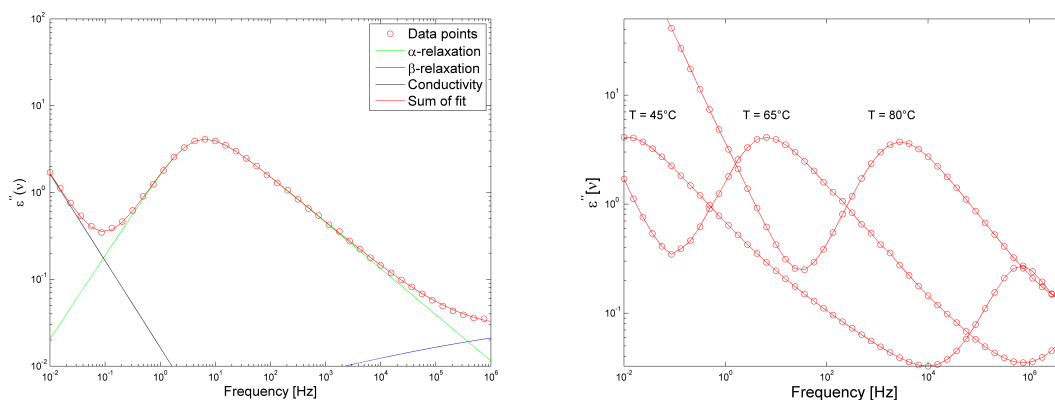


Figure 6.1: *Left: the imaginary part of the permittivity spectrum for felodipine at $T = 60^\circ\text{C}$. Two HN-fitting functions and a conductivity term have been used to fit the spectrum. Right: spectra at three different temperatures, showing how the relaxation processes shift towards higher frequencies as the temperature is elevated.*

The two relaxations found in the spectrum were identified as the α -relaxation and as a β like relaxation. The α -relaxation was expected to have a relaxation time of around 100 s (i.e. 10^{-2} Hz) at 45°C , i.e. at T_g , which can be seen to be the case in the right plot of figure 6.1. To visualize the temperature dependence of the the relaxation times τ_{HN} from the different fitted relaxation processes they were plotted in a relaxation map, as shown in figure 6.2. The relaxation map shows the $\log_{10}(\tau_{HN})$ vs inverse temperature. The relaxation times of the α -relaxation can be fitted by the VFT-equation (3.1) to obtain information on the fragility (D and m parameters) and to extract the temperature where $\tau = 100\text{s}$, i.e. the glass transition temperature.

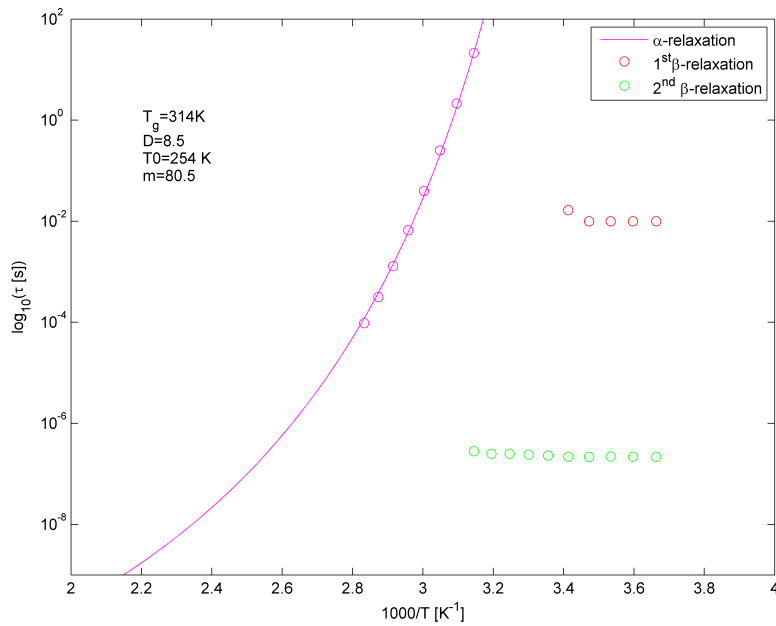


Figure 6.2: Relaxation map for neat felodipine based on the fitted relaxation times τ_{HN} from the imaginary part of the dielectric spectrum. Data points are shown as circles and the solid line is a fit to the VFT-equation.

From this analysis of the α -relaxation times a glass transition temperature of 41 °C was found, which is in good agreement with literature⁴² values and the DSC measurements. Studying the VFT parameters, felodipine can be characterized as a fragile glass former. Two secondary relaxations below T_g were also found. Both processes seem to be temperature independent, see figure 6.2. These processes are not necessarily related to the API, but are more likely to be a result from insufficient electrode contact at low temperatures. A previous study²⁴ on felodipine have shown a secondary relaxation below T_g with an Arrhenius temperature dependence, but this could not be observed here.

6.1.2 Relaxation dynamics of ibuprofen

As with felodipine, neat ibuprofen was analyzed using dielectric spectroscopy and an example of the spectrum at 240K and the resulting relaxation map is shown in figure 6.3. In the left figure, one can see how a relaxation identified as a Debye-relaxation appears as a shoulder on the α -relaxation. The Debye-process exists in several molecular liquids that contain hydrogen-bonding groups^{1,11}. The origin of this relaxation in ibuprofen is however poorly understood but has been attributed to molecular dimer or trimer formation¹¹, i.e. molecular arrangement in groups of two or three.

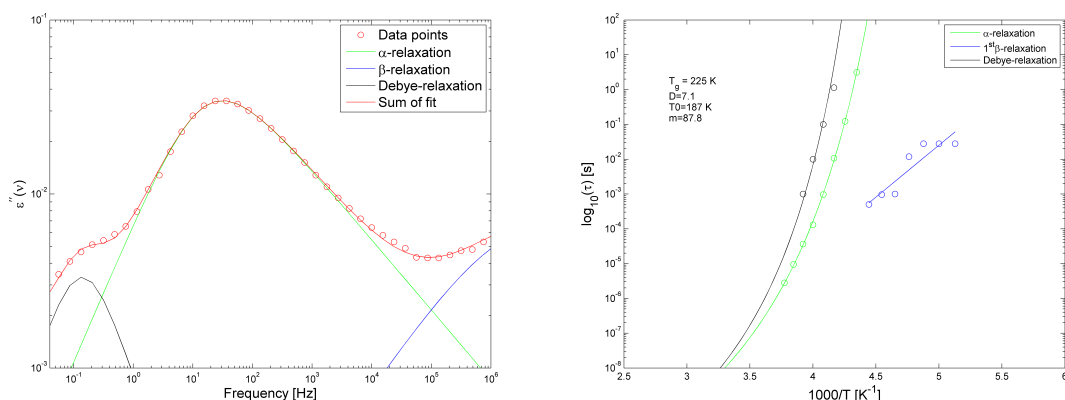


Figure 6.3: *Left: imaginary part of the permittivity spectrum for ibuprofen at $T = 240\text{K}$. The spectrum shows Debye, α , and β processes. Right: relaxation map for ibuprofen.*

From the relaxation map one can identify the α , β and Debye relaxation. The temperature dependence of the α and Debye relaxation times is fitted with the VFT-equation. The identified API T_g based on the extrapolation of the ibuprofen α -relaxation is found to be -48°C , which is in agreement with literature^{8,1} and the DSC results. Previous studies¹¹ have shown the need to fit two different VFT equations to the ibuprofen α -relaxation times but this would be expected to occur at higher temperatures than examined here, thus justifying the use of only one. Furthermore, ibuprofen can be classified as a fragile glass former by the fitted VFT parameters m and D shown in the figure, in good agreement with literature¹¹.

6.1.3 Relaxation dynamics of HPMCAS

As can be seen in the dielectric spectra in figure 6.4 a very large conductivity contribution to the dielectric spectrum was found for neat HPMCAS (both as a powder and solvent casted film). This made fitting extremely difficult and no relaxation map from neat HPMCAS could be determined.

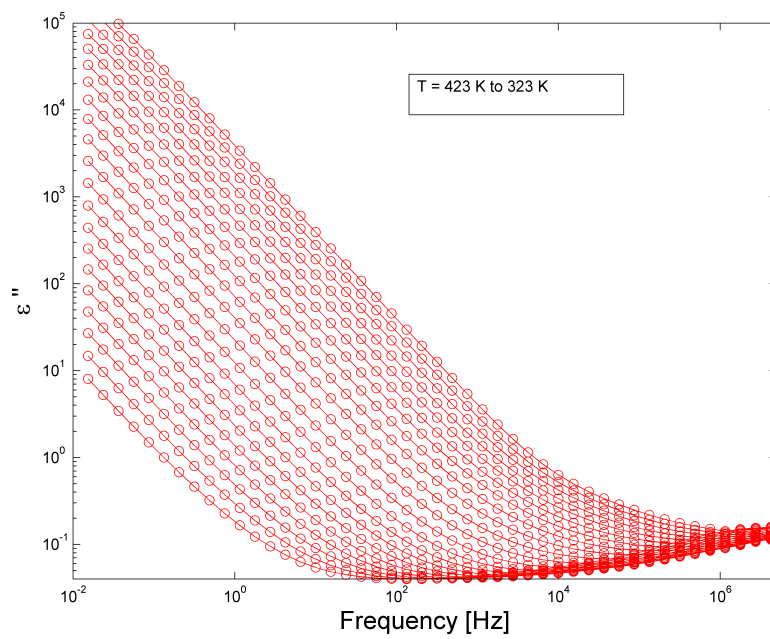


Figure 6.4: Dielectric spectra for HPMCAS powder from 323K - 423K. A very high conductivity contribution masks any contribution from relaxation processes.

6.1.4 Relaxation dynamics of PVP K30

Dielectric spectra from measurements on pressed PVP discs are shown in figure 6.5. Several relaxation processes can be seen, and the data was fitted with three Cole-Cole functions, exemplified to the left in figure 6.6.

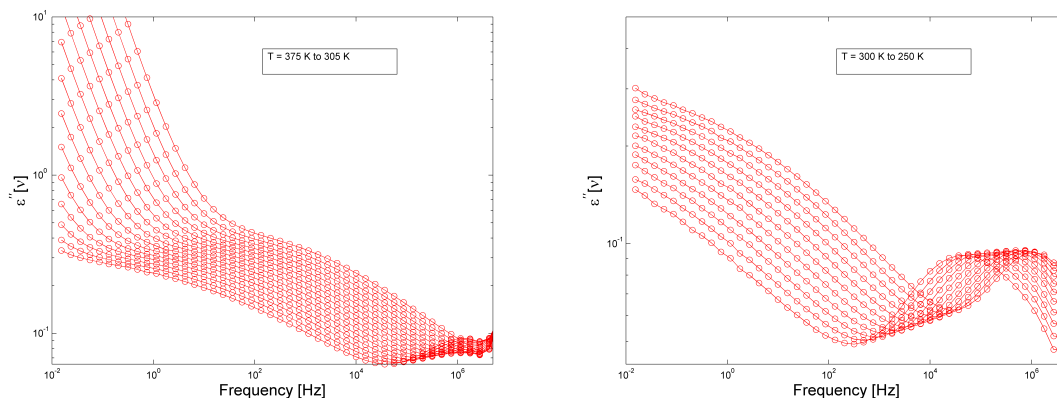


Figure 6.5: The dielectric spectra for PVP powder shown for 250-375 K.

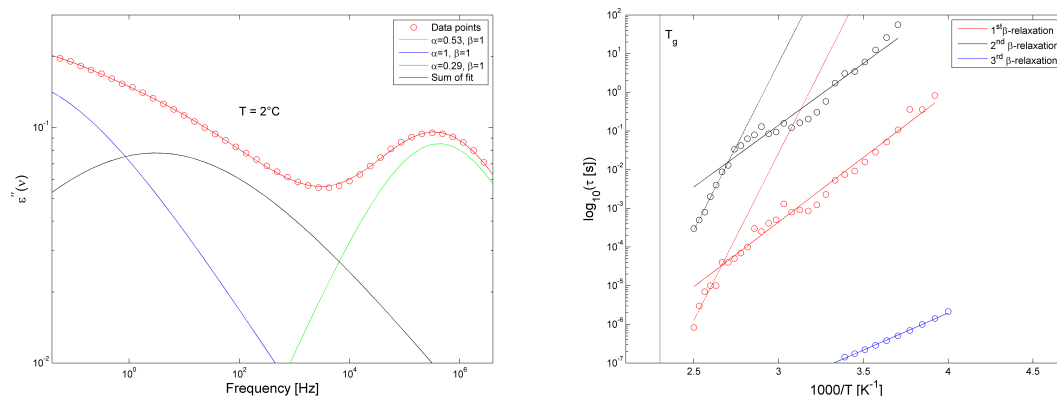


Figure 6.6: Left: imaginary part of the dielectric spectrum for PVP powder at 275K with Cole-Cole fitting function parameters. Right: relaxation map for PVP based on the fitted relaxation times τ_{HN} from the imaginary part of the dielectric spectrum. Data points are shown as circles and the solid lines are fits to the Arrhenius equation. T_g found in the DSC measurements is marked with a vertical line.

The resulting relaxation map is shown to the right in figure 6.6. In the figure, three different β -relaxations can be seen and the two slower processes bend as they approach the predicted glass transition temperature. This behavior has been observed for several systems¹¹, and would therefore indicate the presence of a glass transition at temperatures higher than 375 K, as expected. Previous studies have however displayed the bending at temperatures closer to the glass transition temperature, thus making the indication by the bending uncertain. Because of the tendency of PVP to degrade above and around the glass transition temperature, dielectric measurements

were not made above 400 K. No previous dielectric data of neat PVP K30 could be found in literature, making the evaluation of the origin of the β -relaxations difficult. Literature on other polymers have been studied, but no similar behavior has been found.

6.1.5 Relaxation dynamics of Soluplus®

As with HPMCAS, a massive conductivity contribution in the low frequency part of the dielectric spectrum on Soluplus® made relaxation identification difficult. This is exemplified to the left in figure 6.7, where the spectrum from 20-140°C is shown. The relaxation map is shown to the right in figure 6.7 and two β -relaxations can be found. Literature⁵⁷ has previously been able to identify only one β -relaxation of Soluplus® together with the α -relaxation. The α -relaxation could however not be found because of the large conductivity contribution, and the T_g marked in figure 6.7 is from the DSC measurements.

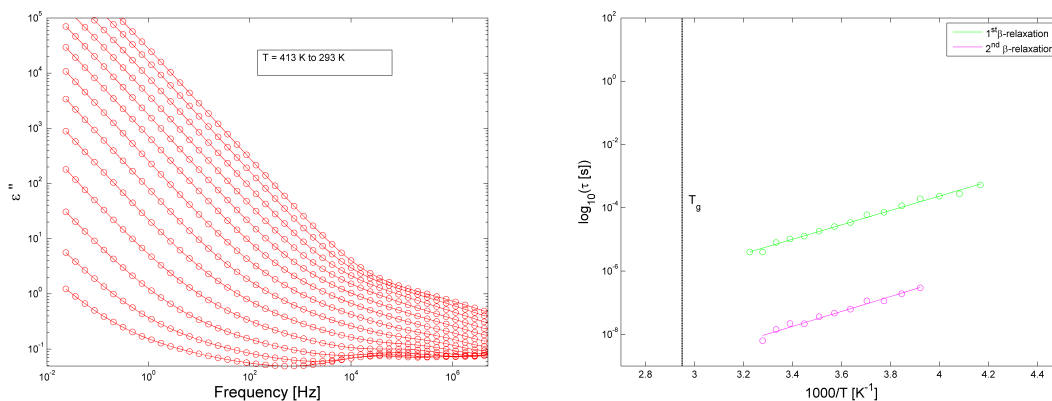


Figure 6.7: *Left: dielectric spectra for Soluplus® in the temperature range 293K - 413K. A very high conductivity contribution masks the relaxation processes, especially at low frequencies. Right: relaxation map for Soluplus®.*

6.2 Solid Dispersion Dynamics

Solid dispersions of the APIs with each of the three polymers were prepared and analyzed. In the following sections both DSC and dielectric spectroscopy results are presented and discussed for each dispersion and finally they are put in comparison to each other. An overview of the preparation results are shown in table 6.2.

Table 6.2: *Summary of the preparation results for the different dispersions of API:polymer.*

	API %	Ibuprofen	Felodipine
HPMCAS	20%	G	G, ✓
	40%	G	G, ✓
	60%	✓	—
	80%	✓	—
PVP K30	20%	✓	x
	40%	✓	x
	60%	✓	x
	80%	✓	—
Soluplus®	20%	✓	—
	40%	✓	—
	60%	✓	—
	80%	✓	—

G : Results available from previous work.

✓: Successful preparation.

x : Unsuccessful preparation.

— : Not prepared.

As shown in table 6.2, solvent casting of felodipine with PVP was not successful for any concentration. A typical sample before annealing is shown to the left in figure 6.8 and as can be seen the film is heterogenous. During annealing it was noticed that it seemed as either solvent or air was trapped within the dispersion as shown by the bubbly appearance to the right in figure 6.8. This type of bubbly behavior could not be circumvented and thus it was concluded that PVP:FD dispersion were not suitable to be prepared by solvent casting.

Solvent casted films for ibuprofen was however successfully prepared with all three polymers. The films were transparent and homogenous, as exemplified in figure 6.9 for PVP:IP20. Because of the limited time available for this thesis and the late arrival of Soluplus®, focus was put on ibuprofen dispersions.

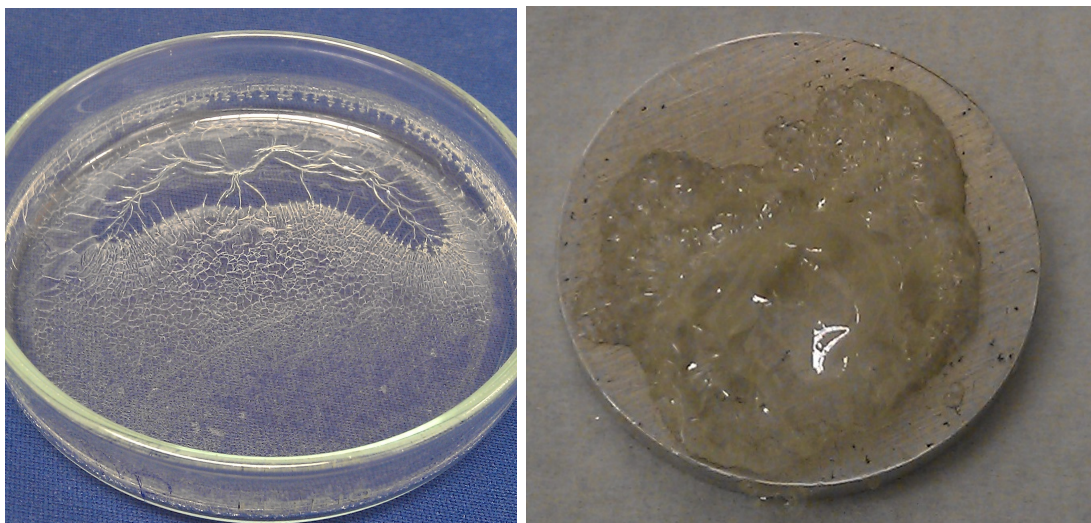


Figure 6.8: *Left: PVP:FD40 casted in glass petri dish before annealing. Right: PVP:FD40 casted onto an electrode and annealed at 60 °C.*

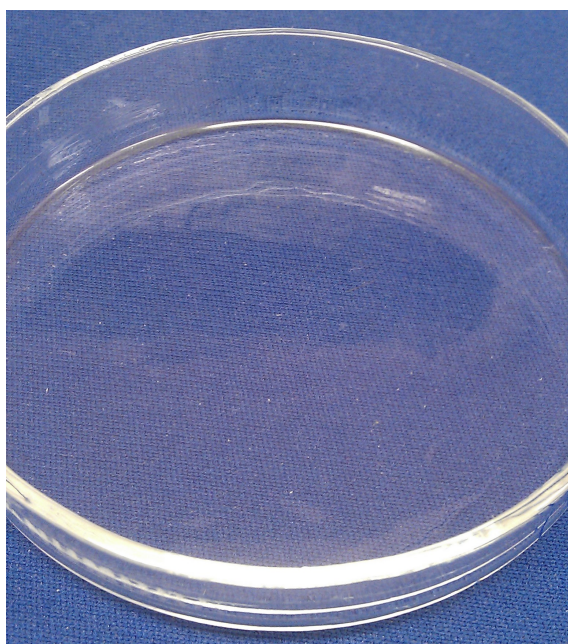


Figure 6.9: *PVP:IP20 solvent casted in petri dish and annealed at 60°C for 15 h.*

6.2.1 Ibuprofen : HPMCAS

The dispersions with ibuprofen and HPMCAS were primarily prepared with high (60% and 80% w/w) API concentration since data for lower concentrations was available from previous work²⁴. The dielectric spectra displayed clear relaxations that could be identified as the α -relaxation and β -relaxation of ibuprofen, seen to the left in figure 6.10. The relaxation maps from the prepared dispersions are shown in figure 6.10 alongside the relaxation map for neat ibuprofen.

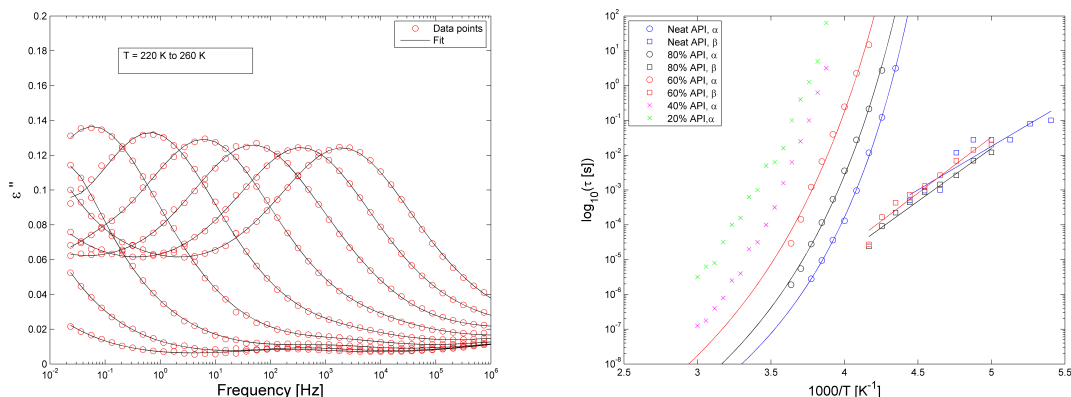


Figure 6.10: Left: *imaginary part of the dielectric spectrum for HPMCAS:IP80 in the temperature range 220-260K. A strong α -relaxation and a weak β -relaxation is observed.* Right: *relaxation maps for neat IP and for sequentially lowered concentrations of API. A clear confinement effect can be seen. Solid lines related to the α -relaxations are fits to the VFT-equation and solid lines related to the β -relaxations are fits to the Arrhenius-equation. *Data shown for 20% and 40% API are previously reported results²⁴*

Figure 6.10 shows that the β -relaxation of ibuprofen is not altered upon polymer confinement as both timescale and activation energy (i.e. the slope of the linear fit) remains approximately the same. Previous studies^{2,30} have claimed a relationship between the activation energy of this so-called Johari-Goldstein β -relaxation process and dispersion stability and this would then suggest an unchanged tendency for recrystallization. The figure also shows a clear confinement effect on the α -relaxation of ibuprofen with increasing polymer content. The relaxation time is increased with around 3 orders of magnitude at 3.7 K^{-1} for 60% API content compared to neat ibuprofen and the T_g is increased to -35°C . A slowing down of the α -relaxation has previously^{9,17,37} been linked to an increase in the crystallization time, thus contradicting the results from the β -relaxation. The α -relaxation results can also be added to previously reported results²⁴ for lower API concentrations as shown in figure 6.10, and the measured α -relaxation confinement follows the trend also reported in that work.

Furthermore, by studying the VFT-fit parameters one can see a clear shift towards a decreasing fragility with increasing polymer content, see table 6.3, in line with previous studies²⁴. Decreasing fragility would then, as explained in section 3.1.2, indicate a pronounced inhibition of crystallization behavior, especially at temperatures close to T_g .

Table 6.3: VFT fitting parameters and calculated T_g for neat IP and dispersions with HPMCAS:IP60 and HPMCAS:IP80. The table shows an increase of T_g and a decrease of fragility with increased HPMCAS content.

	Neat IP	80 % IP	60 % IP
T_g [°C]	-47	-43	-35
D	7.1	9.1	11
T_0 [K]	187	184	182
m	88	76	66

The results from dielectric spectroscopy were compared to DSC measurements on the high concentration API dispersions, shown in figure 6.11. The DSC glass transition temperatures of the dispersions were in good agreement with the extrapolated VFT-fits of the ibuprofen α -relaxations. This indicates that the dispersion dynamics is dominated by the dynamics of ibuprofen.

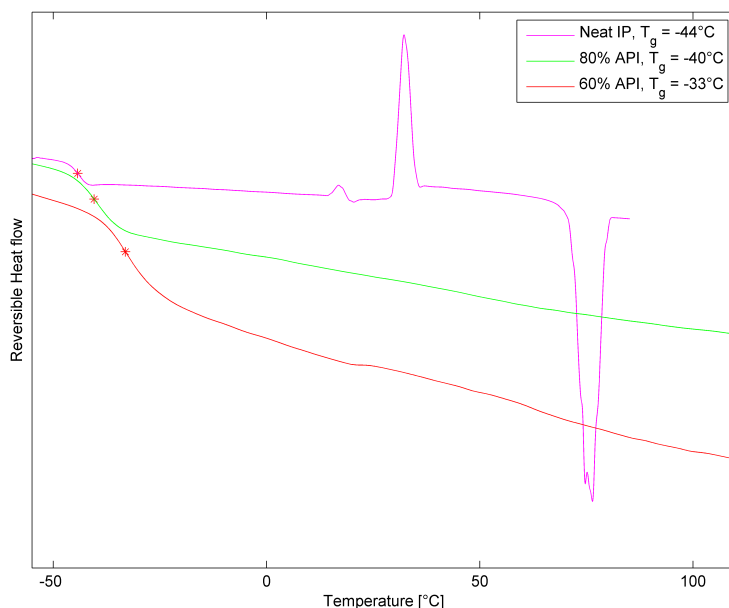


Figure 6.11: DSC thermograms for neat ibuprofen, 80% API and 60% API in HPMCAS.

6.2.2 Ibuprofen : PVP

Solid dispersions with ibuprofen:PVP were successfully prepared for all concentrations as shown in table 6.2. Although, because of the high polymer T_g the films with 20% and 40% API were very brittle and not suitable for dielectric spectroscopy as the contact between the sample and electrodes was insufficient. A dielectric spectrum for 80% ibuprofen in PVP at 240K is shown to the left in figure 6.12. As for neat ibuprofen both an α -relaxation and a Debye-relaxation could be identified

as well as relaxations related to the polymer. At lower temperatures, a secondary relaxation behaving as a β -relaxation was identified as shown to the right in figure 6.12. However, the parameters used to fit the relaxation do not correspond to a Cole-Cole relaxation. This makes the interpretation of this relaxation uncertain. The resulting relaxation map is shown in figure 6.13, and it is seen how the secondary relaxation bends as it approaches the glass transition temperature of -35°C , previously reported for ibuprofen β -relaxations¹. Comparing the figure to neat ibuprofen (figure 6.3) it can also be seen that the Debye-relaxation lies closer in relaxation time to the α -relaxation.

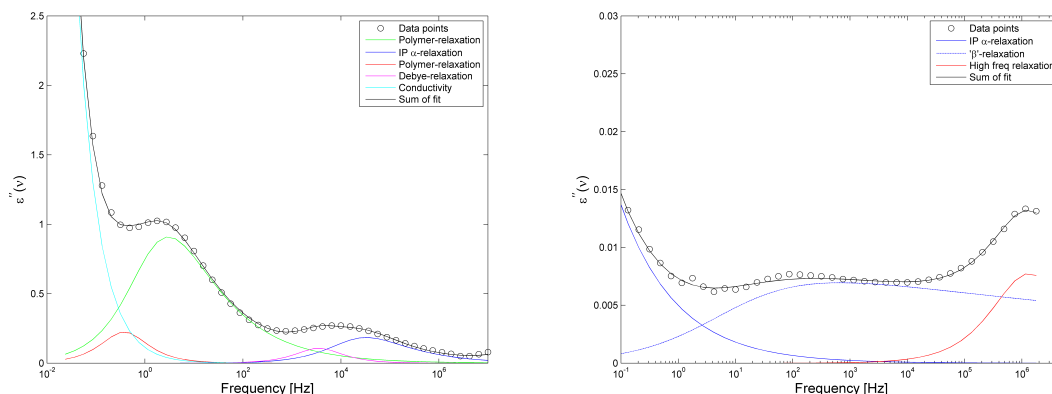


Figure 6.12: *Left: imaginary part of the permittivity spectrum is shown for PVP:IP80 at $T = 240\text{K}$. Right: spectrum at 225K .*

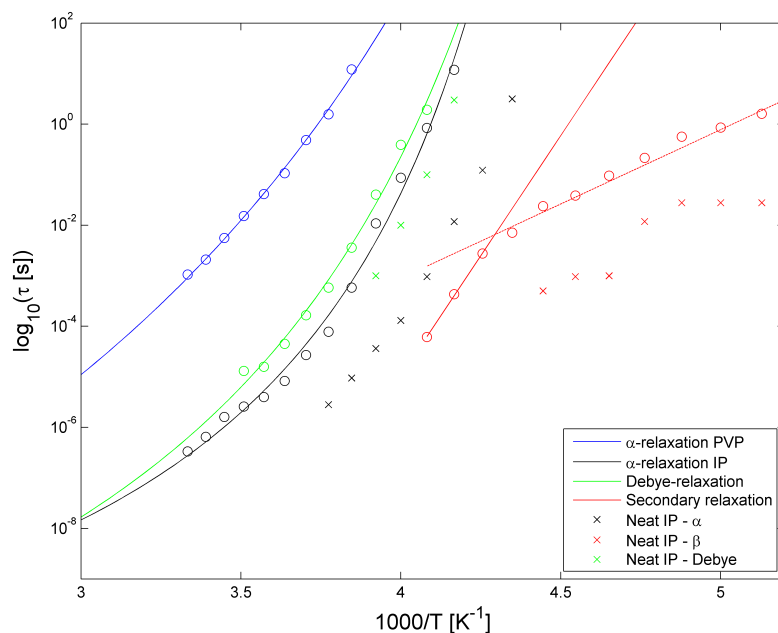


Figure 6.13: *Relaxation maps for PVP:IP80 and neat ibuprofen. The extrapolated glass transition temperature using the VFT fit of the ibuprofen α -relaxation is -34°C .*

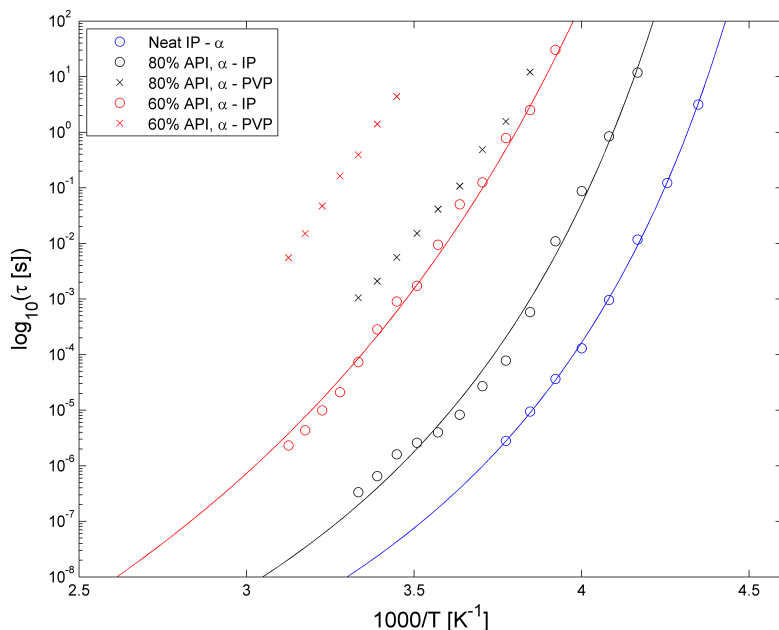


Figure 6.14: Relaxation maps for neat IP (blue), PVP:IP80 (black) and PVP:IP60 (red) are shown. A clear confinement effect is seen for the α -relaxation of ibuprofen.

To fully evaluate the effect of PVP on the dynamics of ibuprofen, the temperature dependence of the α -relaxations for 60% and 80% API are shown in figure 6.14 together with neat ibuprofen as a reference. One can see a clear shift in T_g with increasing polymer concentration and a strong confinement effect. At 60% API the alpha relaxation time increases with around 7 orders of magnitude at 3.7 K^{-1} . By studying the VFT-parameters shown in table 6.4 one can also see that with increasing polymer concentration D increases and m decreases, thus further confirming a less fragile liquid in the dispersions. One should however note that the fitted VFT-equation, which is empirical, deviates from the data points to some degree in the case of confined ibuprofen as can be seen in figure 6.14.

Table 6.4: VFT fitting parameters and calculated T_g for neat IP and dispersions with 60:40 IP:PVP and 80:20 IP:PVP. The table shows an increase of T_g and a decrease of fragility with increased PVP content.

	Neat IP	80 % IP	60 % IP
T_g [°C]	-47	-34	-22
D	7.1	9.2	17
T_0 [K]	187	189	172
m	88	72	52

In the relaxation map in figure 6.13 a slow relaxation for the solid dispersions was identified as the α -relaxation of PVP. This was motivated by the resemblance of the observed relaxations with the behavior of the β -relaxations of neat PVP near

the T_g of neat PVP as previously shown in figure 6.6. It was also motivated by the high strength of the dielectric signal compared to the α -relaxation of ibuprofen. This would then suggest a drastic plasticizing effect of ibuprofen on the polymer, i.e. the polymer softens. The polymer T_g decreases with increasing API content, from 160°C in neat PVP to 8°C and -13°C for 60% API and 80% API respectively.

When comparing the secondary relaxation processes of ibuprofen, an interesting feature can be seen for both the 60% and 80% API dispersions, shown to the left in figure 6.15. Here it seems as if the β -process slows down upon confinement, which can not be seen in the dispersions formed with the other polymers. For the 80% API dispersion however, the observed secondary relaxation is doubted to be a true β -relaxation as discussed earlier. Furthermore, the absence of Debye-relaxations for the 60% dispersion is probably due to that the strong signal from the α -relaxation of the PVP masks the weaker Debye-signal, as shown in the imaginary dielectric spectrum for 60% IP shown to the right in figure 6.15.

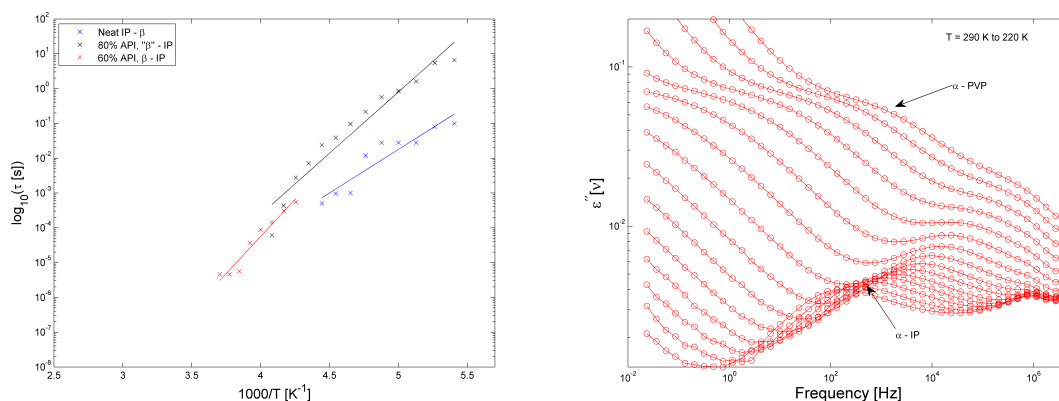


Figure 6.15: Left: β -relaxation in PVP:IP dispersions. Right: imaginary part of the dielectric spectrum for PVP:IP60 from 220K to 290K, showing how the strong polymer relaxation masks any present Debye-relaxation.

To validate the results from the dielectric spectroscopy the dispersions were analyzed using DSC. All API concentrations could be measured in the DSC and the results are shown in figure 6.16.

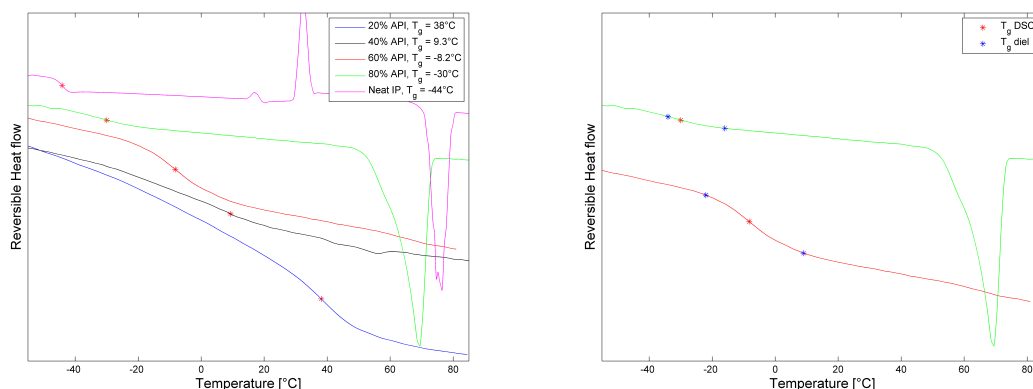


Figure 6.16: *Left: thermograms showing reversible heat flow for IP:PVP ratios and the midpoint T_g is marked for each dispersion. Right: reversible heat flow for 60% and 80% IP in PVP dispersions and the T_g s determined with dielectric spectroscopy are marked with blue crosses. In both figures the respective signals are scaled to better visualize the glass transition and can therefore not be compared in absolute numbers.*

In the figure the respective signals are scaled to better visualize the glass transitions and can therefore not be compared in absolute numbers. The T_g from 60% and 80% dispersions are in good agreement with the dielectric results presented in table 6.4. One can also see a melting endotherm for the 80% dispersion indicating the presence of crystalline ibuprofen within the sample. Furthermore, we can observe an increase of T_g with increasing polymer concentration, as predicted by the Gordon-Taylor equation (3.7). A clear broadening of the glass transition is also seen with increasing polymer concentration which makes T_g determination less accurate. To analyze this broadening the α -relaxation glass transition temperatures for both ibuprofen and PVP from the dielectric measurements are marked to the right in figure 6.16. From the figure it can be seen that the glass transition found with DSC is a mixture of the ibuprofen and PVP α -relaxations from the dielectric measurements. It can also be seen that increasing PVP concentration broadens the T_g of the dispersion and that the T_g seen for high polymeric concentrations will be heavily dominated by the polymer thus making the determination of API T_g difficult.

6.2.3 Ibuprofen : Soluplus®

Dispersions with ibuprofen:Soluplus® were successfully prepared with the solvent casting method and were all possible to study with dielectric spectroscopy. However, as mentioned earlier in 6.1.5, the Soluplus® part of the spectra is difficult to analyze because of the high conductivity contribution and it rendered fitting the spectra for low API concentrations difficult. Examples of the fitted spectra and the resulting relaxation maps for higher API concentrations are shown in figure 6.17 and 6.18.

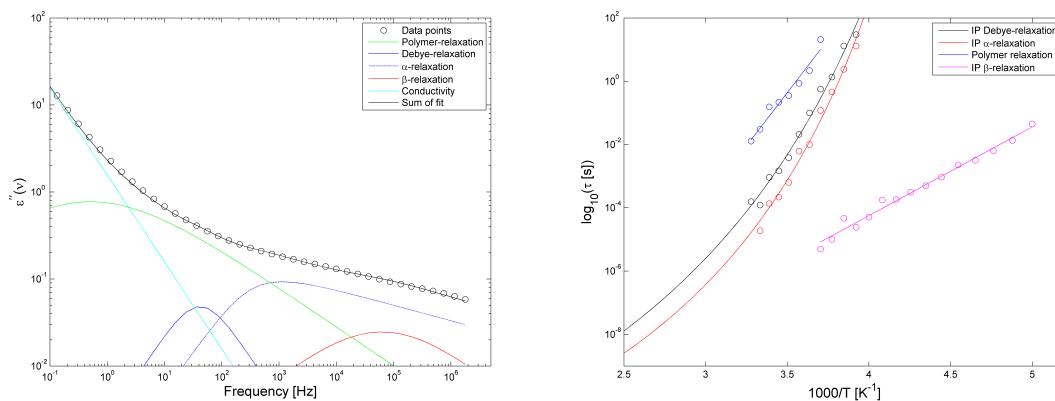


Figure 6.17: Left: *imaginary part of the dielectric spectrum for SOL:IP60 at $T = 285K$. The spectrum shows both Debye, α - and β -relaxation processes for ibuprofen as well as a polymer related relaxation. Right: resulting relaxation map.*

In the SOL:IP dispersions, a clear asymmetrical broadening of the ibuprofen α -relaxation can be seen in figure 6.17 compared to the neat drug (figure 6.3), not seen to the same extent in the other polymer dispersions. The broadening indicates structural heterogeneity of the sample and a wider distribution in molecular size giving rise to a wide distribution in dynamics. A comparison of the confinement effect of the α and β -relaxation of ibuprofen in the polymer can be seen in figure 6.19.

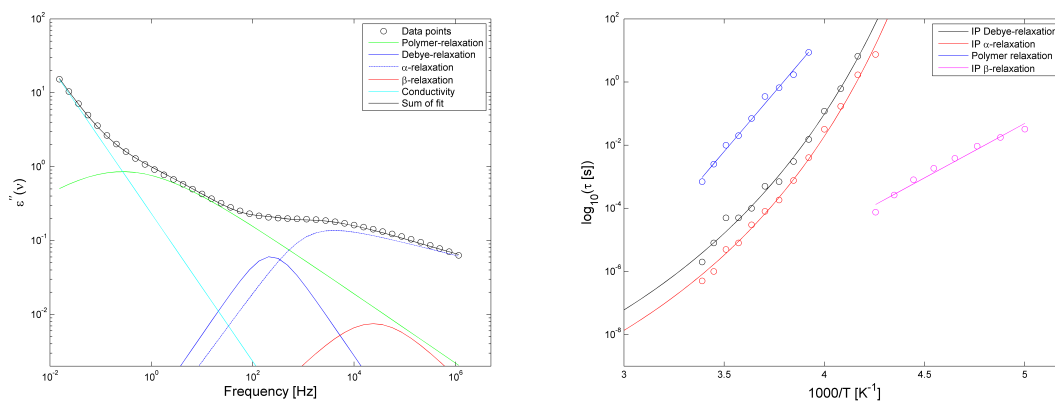


Figure 6.18: Left: *imaginary part of the dielectric spectrum for SOL:IP80 at $T = 265K$. The spectrum shows both Debye, α - and β -relaxation processes for ibuprofen and a polymer related relaxation. Right: resulting relaxation map.*

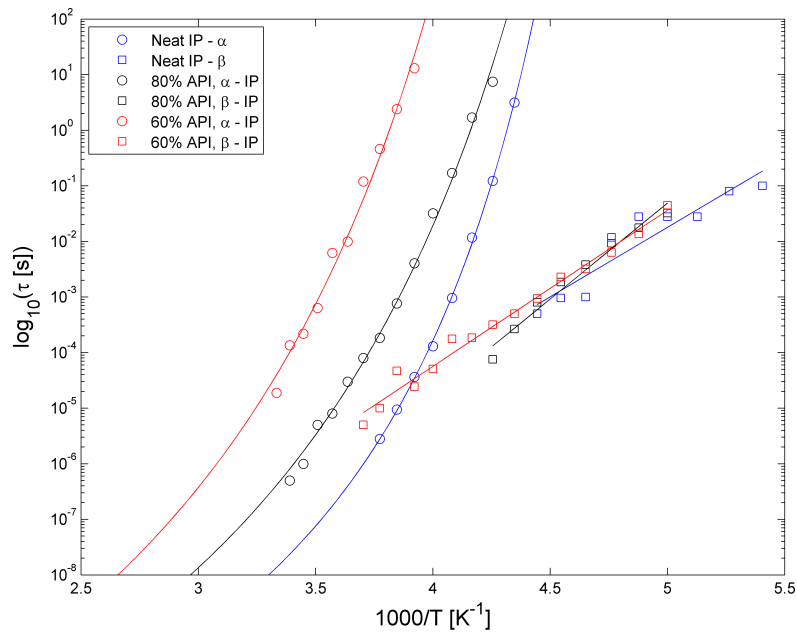


Figure 6.19: Relaxation maps for neat IP (blue), SOL:IP80 (black) and SOL:IP60 (red) are shown. A clear confinement effect is seen for the α -relaxation of ibuprofen.

The figure shows a clear confinement effect of the α -relaxation, having an increase of relaxation time with 5 orders of magnitude at 3.7 K^{-1} . As for HPMCAS dispersions there is no/very small change of the β -relaxation. Furthermore, the dispersions also show a decreased fragility with increasing polymer content as shown in table 6.5.

Table 6.5: VFT fitting parameters and calculated T_g for neat IP and the dispersions SOL:IP80 and SOL:IP60.

	Neat IP	80 % IP	60 % IP
T_g [°C]	-47	-42	-21
D	7.1	12	13
T_0 [K]	190	174	184
m	88	62	57

To confirm the results from the dielectric spectroscopy DSC measurements were made and the results are shown in figure 6.20.

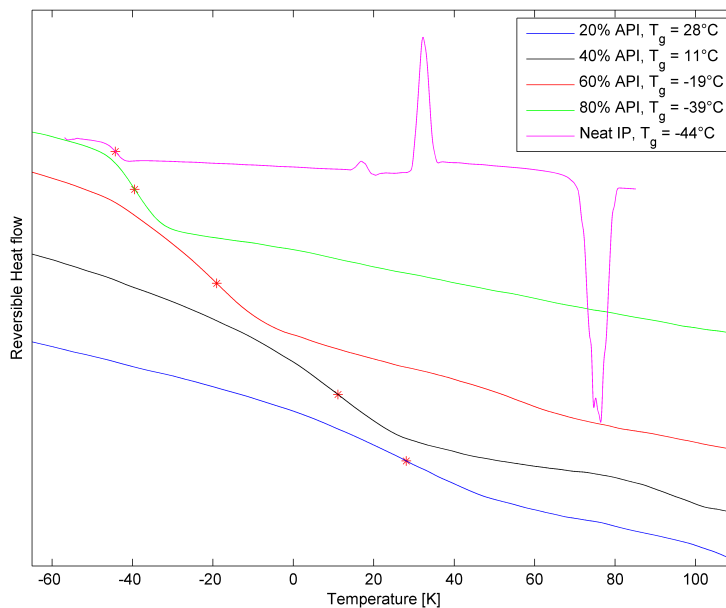


Figure 6.20: *Left: thermograms showing reversible heat flow for different IP:SOL ratios and the midpoint T_g is marked for each dispersion.*

As with the other polymer dispersions, a clear elevation and broadening of the glass transition can be seen with increasing polymer concentration. Also, the glass transition temperatures found for the ibuprofen α -relaxation in dielectric spectroscopy is in good agreement with the DSC data. As for PVP and HPMCAS dispersions however, the DSC T_g is expected to deviate from the dielectric T_g of the API as the polymer concentration increases due to the increasing contribution from polymer dynamics.

6.2.4 Comparison of dynamics in dispersions

To compare the confinement effect on ibuprofen between the three different dispersions, the relaxation maps for all three dispersions (60% and 80% (w/w) API) are shown in figure 6.21 and 6.22 respectively.

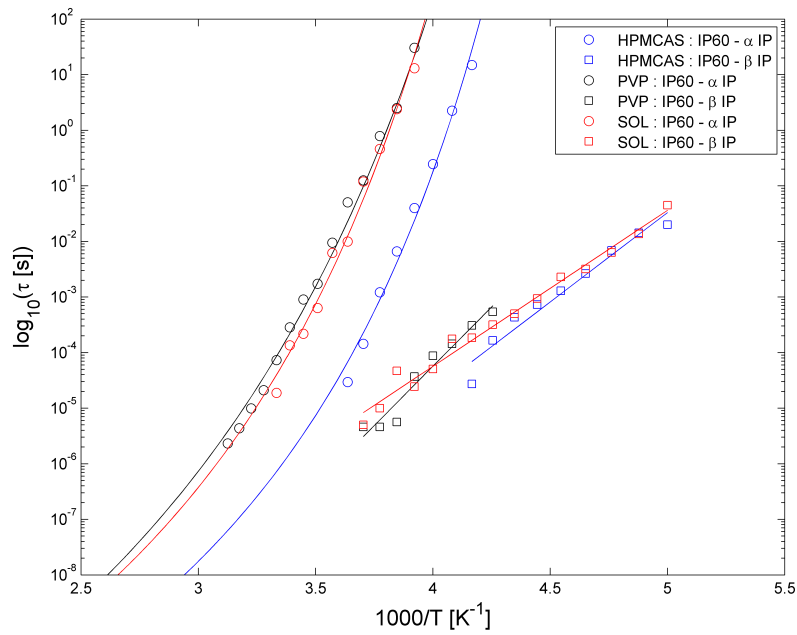


Figure 6.21: Relaxation maps for HPMCAS:IP60, PVP:IP60, and SOL:IP60. The polymeric confinement effect on ibuprofen α -relaxation can be ranked as: $PVP \geq SOL > HPMCAS$. This relationship also holds for the β -relaxation.

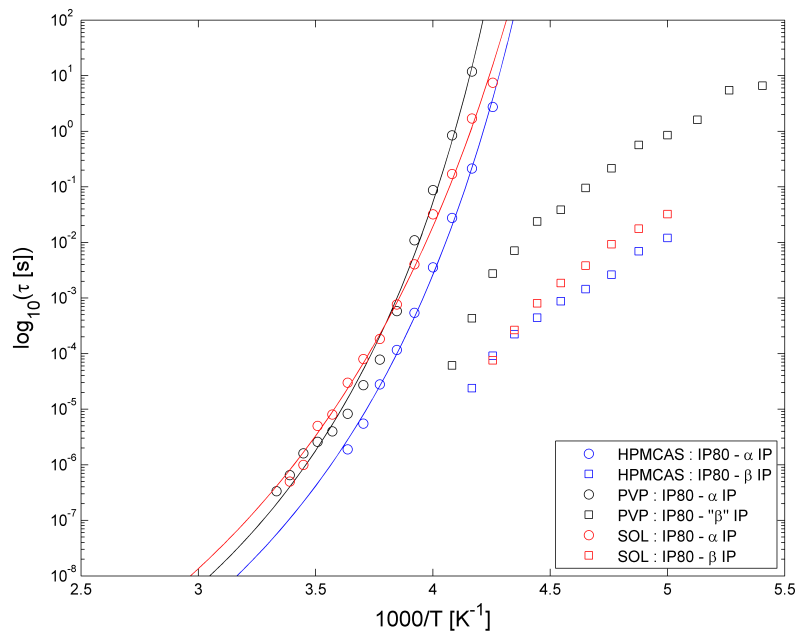


Figure 6.22: Relaxation maps for HPMCAS:IP80, PVP:IP80, and SOL:IP80. The polymeric confinement effect on ibuprofen α -relaxation can be ranked as: $PVP \geq SOL > HPMCAS$.

From figure 6.21 and 6.22 it can be seen that the polymeric confinement effect on the

ibuprofen α -relaxation can be ranked as: PVP \geq SOL>HPMCAS. The glass transition temperature of the neat state polymers does therefore not effect the polymer's ability to confine ibuprofen. Since the α -relaxation is directly linked to the mobility of the ibuprofen molecules, the same relationship holds for mobility inhibition. As previously mentioned this would then, based on previous studies, suggest the same relationship in the crystallization inhibition ability. This relationship also holds for the ibuprofen glass transition temperatures calculated from the VFT fits to the relaxation maps, as summarized in table 6.6.

Table 6.6: *Calculated ibuprofen T_g from VFT fits to the dielectric relaxation maps for dispersions of ibuprofen with HPMCAS, PVP K30 and Soluplus respectively.*

	80 % IP	60 % IP
HPMCAS	-43	-34
PVP K30	-34	-22
Soluplus	-42	-21

6.3 Crystallization Inhibition of Solid Dispersions

To evaluate the crystallization inhibition property of each polymer, two measurement protocols were initially followed: i) The sample was kept at 85°C ($\sim 10K > T_g$) for 30 minutes, then at -60°C for 20 min and then raised to 0°C, ii) sample kept at 85°C for 30 minutes, then lowered to 0°C. Dispersions with 80% API content for all three polymers were prepared as less API content rendered crystallization monitoring impossible. The dispersions with 20% and 40% API content did not crystallize on the timescale of months when stored in air and at room temperature. The monitoring temperature was based on the moderate molecular mobility of ibuprofen in both the neat state and in the dispersions at this temperature as seen in figure 6.23. The peak frequencies of the ibuprofen α -relaxation are marked with vertical lines.

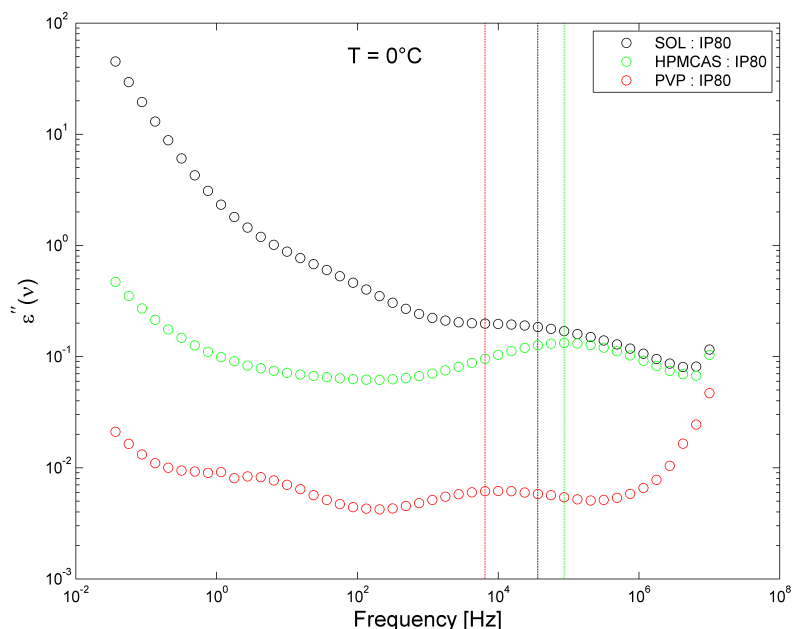


Figure 6.23: Imaginary part of the dielectric spectrum at 0°C for SOL:IP80, HPMCAS:IP80 and PVP:IP80. The ibuprofen α -relaxation peak frequencies are marked with vertical lines.

The resulting spectra and the analysis for neat ibuprofen are shown in figure 6.24. Data for the dispersions can be found in section A.3. A summary of kinetic parameters for both neat ibuprofen and all three dispersions with both measurement protocols are shown in table 6.7.

6. Results & Discussion

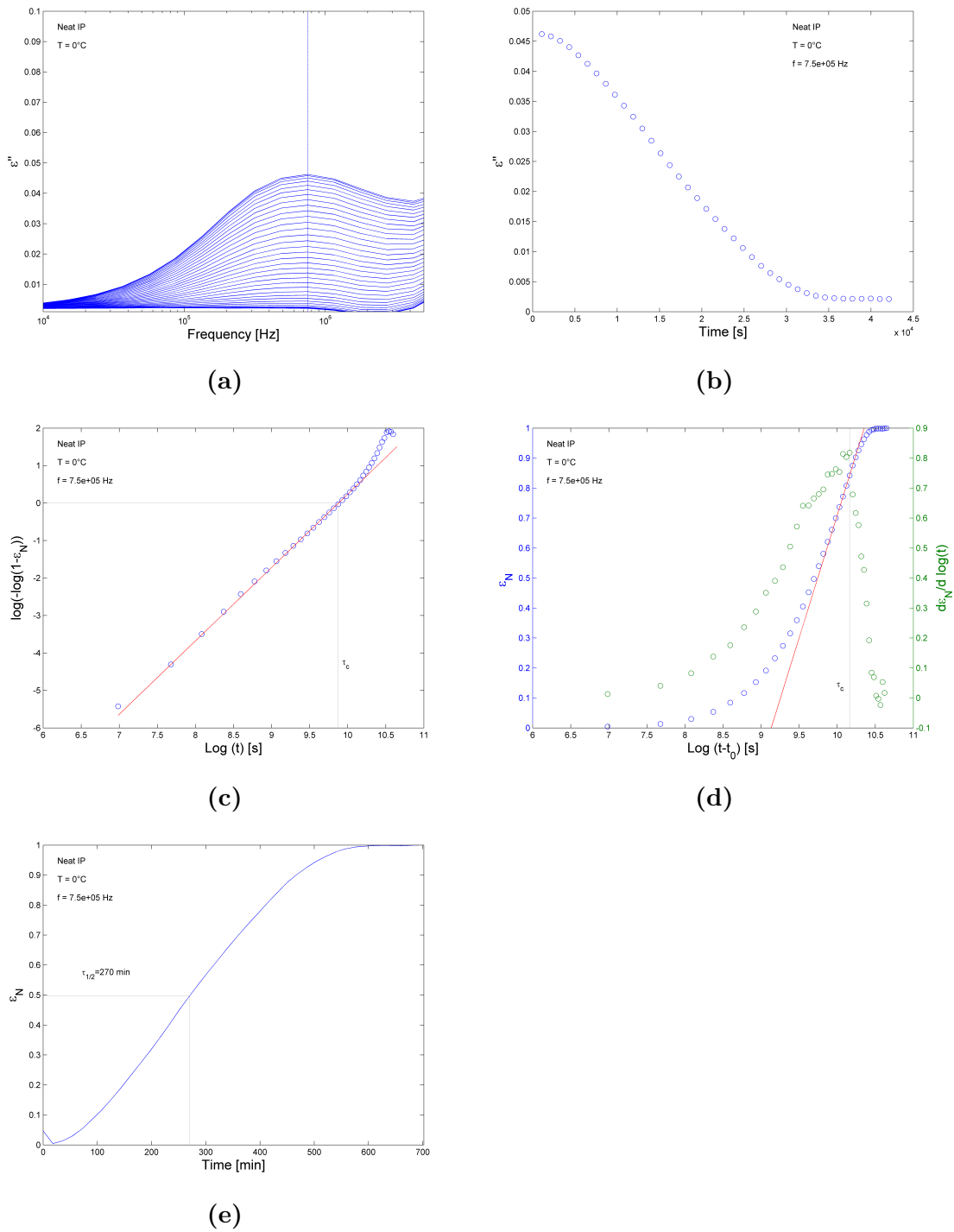


Figure 6.24: a) Dielectric spectrum of ibuprofen following measurement protocol *i*, at 0 °C monitored for 24 h. The analyzed frequency ($7.5e5$ Hz) is marked with the vertical line. b) Strength of the dielectric signal at $7.5e5$ Hz vs time. c) Avrami plot. d) Avramov plot marking the crystallization timescale τ_c . e) The normalized dielectric signal vs time where the halfpoint crystallization time $\tau_{1/2}$ is marked.

Table 6.7: *Crystallization kinetics parameters for neat ibuprofen and dispersions with 80% ibuprofen for the two different measurement protocols.*

		T [°C]	Avrami n	Avramov n	Avramov τ_c [h]	t_0 [h]	$t_{1/2}$ [h]
i)	Ibuprofen	0	1.95	2.20	7.2	0	4.5
	HPMCAS:IP	0	1.82	1.59	11.4	0	12
	PVP:IP	0	-	-	-	> 40	> 40
	SOL:IP	0	-	-	-	~50	> 50
ii)	Ibuprofen	0	1.73	1.71	4.2	0	4.2
	HPMCAS:IP	0	-	-	-	~50-70	50-125
	PVP:IP	0	-	-	-	100-250	100 - 250
	SOL:IP	0	-	-	-	> 55	> 55

The n parameters of neat ibuprofen following protocol i is in very good agreement with literature data which shows $n = 2.2 - 2.3^1$. However, τ_c and t_0 can not be compared as the measurements in literature were made at lower temperatures. The inhibitory effect of the polymer can be clearly seen as crystallization is delayed for all dispersions and both measurement protocols. Interestingly, the dispersion with Soluplus had around 5% signal strength decrease after 50 h while ibuprofen in HPMCAS had fully crystallized after the same time using protocol i . This despite having similar API glass transition temperature (table 6.6), and a significantly lower polymer glass transition temperature of Soluplus as well as ability to form hydrogen bonds. This demonstrates the insufficiency of molecular mobility as a predictor of physical stability.

Interesting to note is also the significant decrease of the n parameter when following protocol ii . This decrease signifies a crystallization behavior limited to fewer dimensions, which is also shown for the API confined in the HPMCAS polymer with protocol i . In the polymer this behavior is expected since the confinement of the pharmaceutical limits the mobility and growth patterns of the crystals. Why this is seen for neat ibuprofen is however unclear. The second measurement protocol also effected the crystallization inhibition property of the HPMCAS:IP dispersion as it significantly increased crystallization time, although full crystallization could still be seen after around 5 days (A.3). It further increased the crystallization onset time for the SOL:IP dispersion to exceed the experimental timescale.

As can be seen in the table and in section A.3, the PVP:IP dispersion did crystallize at 0°C after >100 h for measurement protocol ii . The sample was stored in air at room temperature inbetween the measurements at 0°C, and the crystallization could therefore be induced by the thermal stress on the sample. Using measurement protocol i , no sign of crystallization was seen up to 40 h, but they were not stored for further measurements as the equipment was needed for other measurements.

To analyze the influence of ibuprofen α -relaxation times on crystallization, the PVP:IP dispersion was monitored for crystallization at room temperature (21°C). This temperature was selected as the ibuprofen α -relaxation peak frequency approximates the frequency peak for neat ibuprofen at 0°C, as can be seen in figure

6.25.

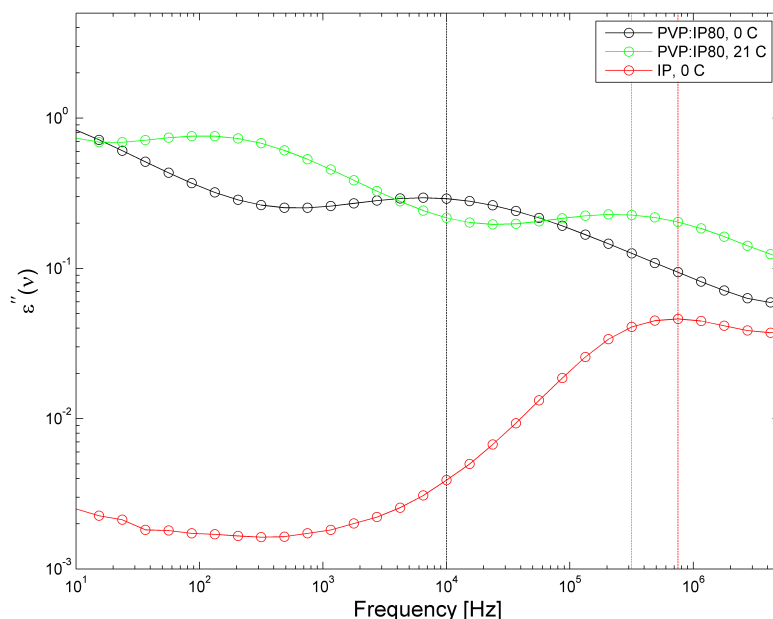


Figure 6.25: *Imaginary part of the dielectric spectrum for PVP:IP80 at 0°C and 21°C and for neat ibuprofen at 0°C. Ibuprofen α -relaxation peak frequencies are marked with vertical lines.*

The imaginary part of the dielectric spectrum and the strength of the dielectric signal versus time is shown in figure 6.26. Crystallization was inhibited for >400 hours, thus the correlation between the ibuprofen α -relaxation times and crystallization is weak. This absence of a correlation between ability to crystallize and the α -relaxation time-scale has been reported before for ASDs in the supercooled region², although several studies have claimed a strong relationship both above and below T_g . The sample was stored in air and at room temperature inbetween measurements, thus excluding the possibility that the dispersion measured with protocol *ii* crystallized because of the storage conditions, but rather due to the thermal stress. Summarizing the crystallization inhibition investigation one can conclude that the T_g of the polymer does not effect the polymer's ability to inhibit crystallization of ibuprofen. Furthermore a higher mobility of the API is not necessarily worse for crystallization inhibition. Therefore other types of mechanisms must be responsible for the inhibition of crystallization.

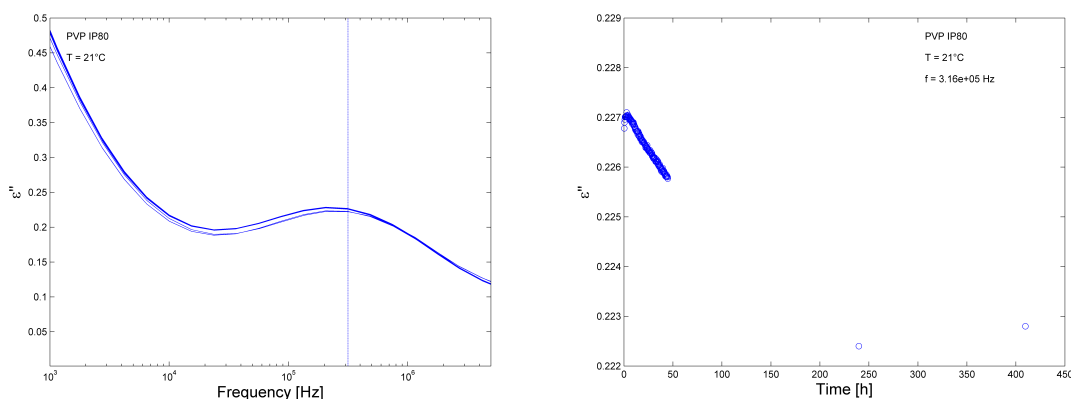


Figure 6.26: a) Dielectric spectrum of PVP:IP80 at 21 °C monitored for 44 h using protocol ii and subsequent measurements after 240 h and 410 h. The analyzed frequency ($3.2e5$ Hz) is marked with the vertical line. b) Strength of the dielectric signal at $3.2e5$ Hz vs time. A very small decrease (<1%) in signal strength is shown, signalling no crystallization.

6.4 Stabilization Mechanisms

As shown in the previous section, the anti-plasticization effect of the polymer on the API does not explain the drastically increased crystallization times. The dispersions were therefore analyzed using FTIR (Fourier Transform InfraRed) spectroscopy. FTIR spectroscopy analyzes the infrared absorption spectra of a sample over a wide spectral range, thus giving information about intramolecular and intermolecular structures. The FTIR measurements were performed in a Bruker FRA106 spectrometer in an ATR mode (Golden Gate diamond crystal). The spectral resolution was 4 cm^{-1} .

To be able to analyze the confinement effect on ibuprofen, amorphous and crystalline ibuprofen were measured as reference and the resulting spectra are shown in figure 6.27. The figure shows that there are strong similarities between the spectra from the crystalline and the amorphous samples, although the peaks in the spectrum from the amorphous sample are broader and lower in intensity. In the figure, the band at 1700 cm^{-1} originates from the hydrogen bonded carboxylic C=O stretching vibration as previously found in literature^{39,50}. This band is shifted to lower wavenumbers compared to the free C=O stretching band as marked in the figure. Literature also suggest that the bands at $2900\text{-}3400 \text{ cm}^{-1}$ originates from a broad band from both hydrogen bonded O-H group covered by intense C-H stretching vibrations. A free O-H stretching vibration at 3536 cm^{-1} is absent from the spectra. It can thus be concluded that the ibuprofen molecules exist predominantly in the form of hydrogen bonded aggregates in both phases. It should be noted that the behavior of a very sharp drop in intensity above 1700 cm^{-1} comes from the experimental setup and the properties of the ATR crystal. This behavior would ideally be solved by using a crystal with higher index of refraction but when this was used the signal to noise ratio was too low to obtain useful spectra.

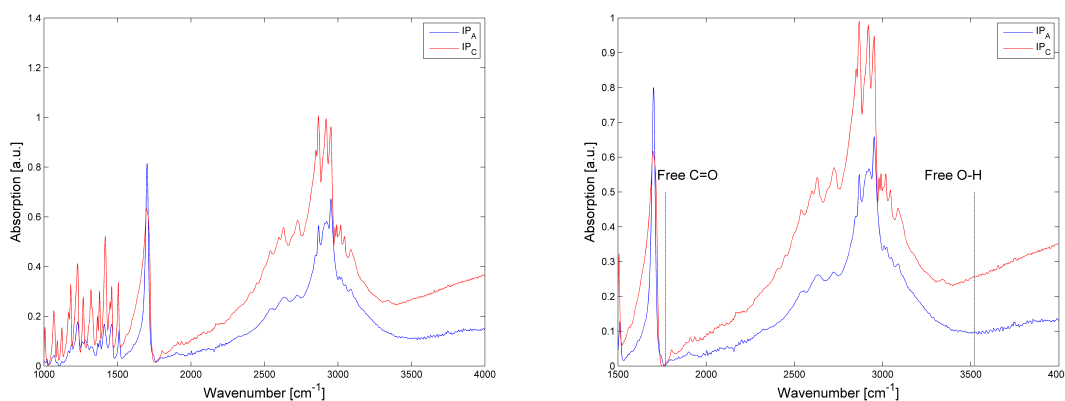


Figure 6.27: Left: FTIR spectra from amorphous and crystalline ibuprofen. Left: enlargement of the region $1500\text{--}4000\text{ cm}^{-1}$ and the characteristic frequencies for free C=O and O-H stretching vibrations are marked with vertical lines.

FTIR spectra for each of the three different dispersions are shown below in figure 6.28-6.30. Spectra of the neat polymers were in good agreement with literature^{36,40,56} and are shown in the figures as reference.

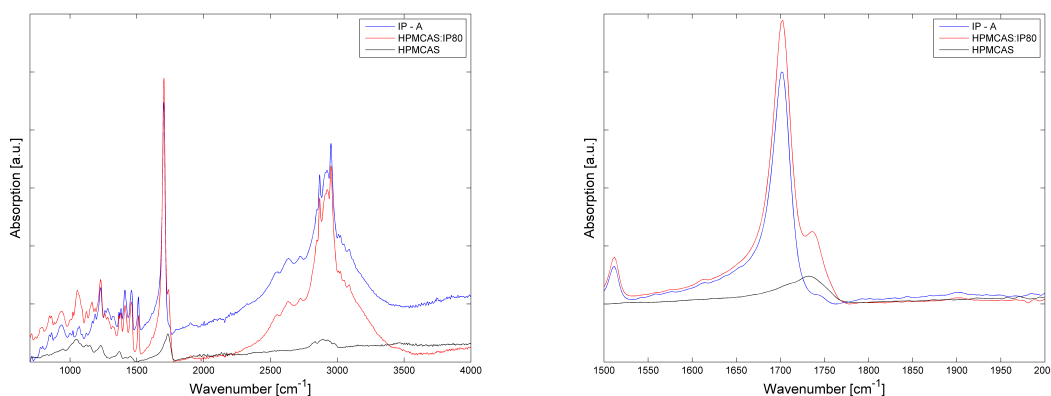


Figure 6.28: Left: FTIR spectra from amorphous ibuprofen, neat HPMCAS and HPMCAS:IP80 dispersion. Right: enlargement of the spectra in the region $1000\text{--}1500\text{ cm}^{-1}$.

From figure 6.28 it can be seen that the spectrum from the dispersion is more or less a sum of the two individual components suggesting that no intermolecular interactions take place. HPMCAS has previously³⁷ been proven to be able to form hydrogen bonds with other APIs, so the reason behind the absence of hydrogen bonding with ibuprofen is unclear.

It can be seen in figure 6.29(PVP:IP80) that the dispersion shows different behaviour than the individual components. This is especially seen to the right as the C=O stretch of the polymer shifts towards lower wavenumbers as well as increases in intensity, indicating hydrogen bonding with the API³⁶. The C=O stretch of the ibuprofen carbonyl group is slightly shifted to higher wavenumbers indicating that

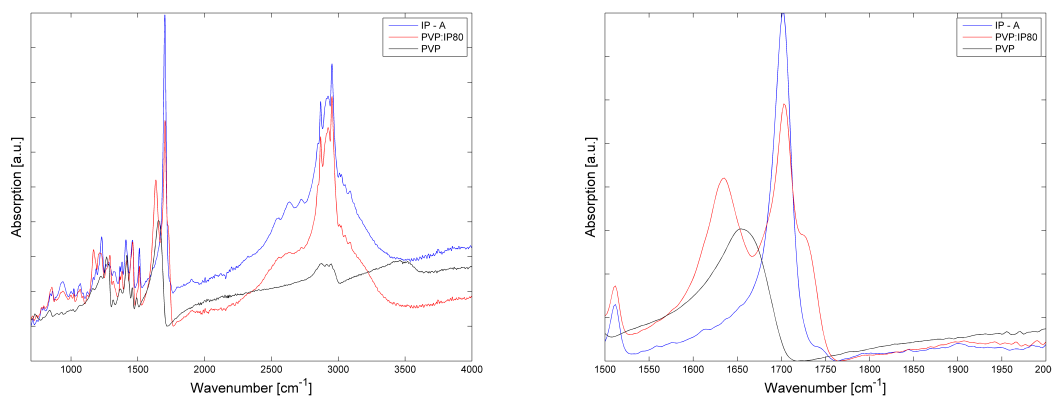


Figure 6.29: To the left, the FTIR spectra for amorphous ibuprofen, neat PVP and PVP:IP80 dispersion are shown. To the right, an enlargement of the spectra from $1000\text{--}1500\text{ cm}^{-1}$ is shown.

the drug molecules does not interact with its hydroxyl group to the same extent, thus further implying hydrogen bonding to the polymer. The same type of behaviour was also seen for SOL:IP80 dispersions, as seen in figure 6.30.

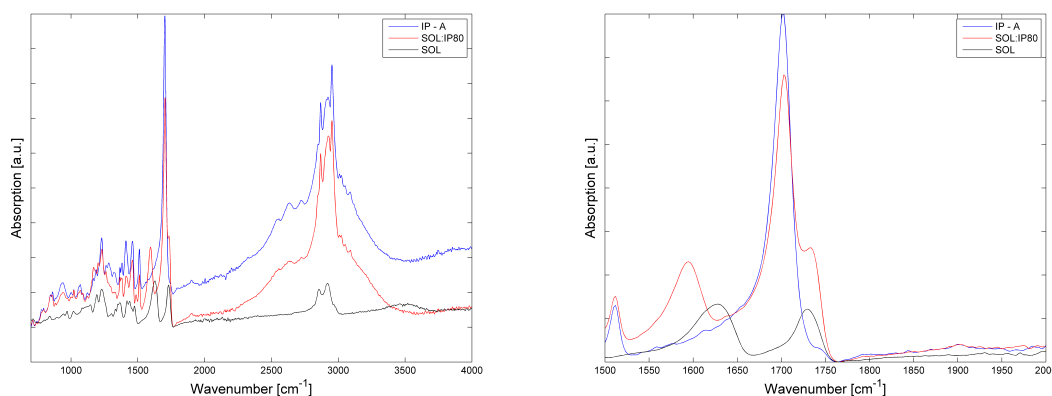


Figure 6.30: To the left, the FTIR spectra for amorphous ibuprofen, neat SOL and SOL:IP80 dispersion are shown. To the right, an enlargement of the spectra from $1000\text{--}1500\text{ cm}^{-1}$ is shown.

In figure 6.30, the two bands for pure SOL located at 1733 cm^{-1} and 1634 cm^{-1} are the carbonyl bands of the vinyl acetate (VAc) and vinyl caprolactam (VCL) respectively. Previous literature³⁹ has shown that the VCL band splits into two separate bands upon forming a dispersion with ibuprofen. The shifted band at 1595 cm^{-1} can be assigned to the VCL component that hydrogen bonds to the drug, thus further indicating that the dimeric form of the drug is destroyed and that the drug instead binds to the polymer. As for the PVP dispersions, a slight shift to higher wavenumbers for the ibuprofen carbonyl peak further motivates this hypothesis. This suggests that a fraction of the drug is molecularly dissolved within the dispersion while most of it is still in amorphous drug rich region.

Based on these results, a clear connection can be seen between the crystallization inhibition properties and its ability to form hydrogen bonds with the API. This would then serve as the main mechanism behind the stabilization as neither the mobility nor the glass transition temperature display such strong correlation.

7

Conclusion

This final section starts with summarizing the key findings of this thesis and then gives an outlook on possibilities for future work.

7.1 Summary

The neat components were initially analyzed using DSC and dielectric spectroscopy and there was good agreement with literature, where literature data could be found. Dispersions with ibuprofen were successfully prepared for all three polymers, although at low API concentrations significant difficulties were encountered in the process of extracting the film from the mold for PVP. The dynamics of ibuprofen were monitored using dielectric spectroscopy and all three polymers exerted a confinement effect on the API, where $\text{PVP} \geq \text{SOL} > \text{HPMCAS}$. This held true for both the α and β -relaxations of ibuprofen at both 60% and 80% (w/w) API.

Dispersions with felodipine were successfully prepared with HPMCAS but failed at all concentrations with PVP. As the solvent evaporated it created bubbles that suggested entrapment of air and solvent within the dispersion. Because of the late arrival of Soluplus®, felodipine was abandoned in favor of deeper studies on ibuprofen.

The kinetics of crystallization were monitored for dispersions with 80% API with the three different polymers respectively. The crystallization inhibition property of the polymer ranked as $\text{PVP} \geq \text{SOL} > \text{HPMCAS}$, where PVP dispersions stayed stable in room temperature over a timescale of weeks. Crystallization measurements showed that the correlation between the API mobility timescale within the dispersion and crystallization was weak, and that the polymeric glass transition temperature did not correlate with the crystallization inhibition property. A more plausible mechanism behind the crystallization inhibition was found using FTIR spectroscopy where it was found that both PVP and SOL hydrogen bond to ibuprofen while HPMCAS do not. The origin of this behavior is however unclear.

7.2 Outlook

The results of this thesis adds to the complexity of understanding the mechanisms behind the stabilization effect in amorphous solid dispersions. It shows that it is possible to study the dynamics of the API confined within the dispersion and also that the crystallization kinetics are possible to monitor. Increasing the API content

7. Conclusion

would be of interest to stress crystallization and do a more complete characterization of each polymer's individual property to inhibit crystallization. Furthermore, more studies aimed at linking the molecular structure of the APIs and polymers to the underlying stabilization mechanisms would be of great interest.

Bibliography

- [1] Adrjanowicz K. et al., *Dielectric relaxation and crystallization kinetics of ibuprofen at ambient and elevated pressure*, J Phys Chem B 114 (2010) 6579–6593.
- [2] Alie J. et al., *Dielectric study of the molecular mobility and the isothermal crystallization kinetics of an amorphous pharmaceutical drug substance*, J Pharm Sci 93 (2004) 218-233.
- [3] Al-Obaidi, H., Buckton, G., *Evaluation of grisefulvin binary and ternary solid dispersions with HPMCAS*, AAPS PharmSciTech 10 (2009) 1172-1177.
- [4] Angell, C.A., *Formation of glasses from liquids and biopolymers*, Science 267 (1995) 1924-1935.
- [5] Aso Y., Yohioka S., *Molecular mobility of nifedipine-PVP and phenobarbital-PVP solid dispersions as measured by ¹³C NMR spin-lattice relaxation time*, J Pharm Sci 95 (2006) 318-325.
- [6] Aulton M.E., *Pharmaceutics - The science of dosage form design*, 2nd Ed, Churchill Livingstone, London (2002).
- [7] Avramov I., Avramova K., Russel C., *New method to analyze data on overall crystallization kinetics*, J Cryst Growth 285 (2005) 394-399.
- [8] Baird J.A., Taylor L.S. *Evaluation of amorphous solid dispersion properties using thermal analysis techniques*, Adv Drug Delivery Rev 64 (2012) 396–421.
- [9] Bhardwaj S.P. et al., *Mechanism of amorphous itraconazole stabilization in polymer solid dispersions: role of molecular mobility*, Mol Pharm 11 (2014) 4228-4237.

- [10] Böhmer R. et al, *Nonexponential relaxations in strong and fragile glass formers* The Journal of Chemical physics 99 (1993) 4201-4209.
- [11] Bras A.R. et al., *Molecular motions in amorphous ibuprofen as studied by broadband dielectric spectroscopy*, J Phys Chem B 112 (2008) 11087-11099.
- [12] Brush S. G., *Theories of liquid viscosity*, Chem Rev 62 (1962) 513–548.
- [13] Chou W.L., Riegelman S., *Oral absorption of griseofulvin in dogs: increased absorption via solid dispersions in polyethylene glycol 6000*, J Pharm Sci 59 (1970) 937-942.
- [14] Couchman P.R., Karasz F.E., *Classical thermodynamic discussion of effect of composition on glass-transition temperatures*, Macromolecules 11 (1978) 117–119.
- [15] Cowie J.M.G., Arrighi V., *Polymers: Chemistry and physics of modern materials*, 3rd Ed, CRC Press, New York (2008).
- [16] D'Amore A., Kenny J.M., Nicolais L., *Dynamic-mechanical and dielectric characterization of PEEK crystallization*, Polym Eng Sci 30 (1990) 314-320.
- [17] Dantuluri A.K.R. et al., *Role of α -relaxation on crystallization of amorphous celecoxib above T_g probed by dielectric spectroscopy*, Mol Pharm 8 (2011) 814-822.
- [18] Debye P., Ver Deut Phys Gesell 15 (1913) 777; reprinted 1954 in collected papers of Peter J.W. Debye Interscience, New York.
- [19] Di L., Kerns E.H., Carter G.T., *Drug-like property concepts in pharmaceutical design*, Curr Pharm Des 15 (2009) 2184–2194.
- [20] Dudognon E. et al., *Evidence for a new crystalline phase of racemic ibuprofen*, Pharm Res 25 (2008) 2853-2858.
- [21] Dyre J.C , *Colloquium: The glass transition and elastic models of glass-forming liquids*, Review of Modern Physics 78 (2006) 953-968.

-
- [22] Fahr A., Liu X., *Drug delivery strategies for poorly water-soluble drugs*, Expert Opin Drug Delivery 4 (2007) 403-416.
- [23] Foreman, J., Sauerbrunn, S.R., Marcozzi, C.L., *Exploring the sensitivity of thermal analysis techniques to the glass transition*, Retrieved at http://www.tainstruments.co.jp/application/pdf/Thermal_Library/Applications_Briefs/TA082.PDF, 2016-01-27.
- [24] Ferrand-Drake del Castillo, G. , *To be published*.
- [25] Gashi Z. et al., *Differences in the interaction between aryl propionic acid derivatives and poly(vinylpyrrolidone) K30: a multi-methodological approach*, J Pharm Sci 98 (2009) 4216-4228.
- [26] Goldberg, A.H., Gibaldi, M., Kanig, J.L., *Increasing dissolution rates and gastrointestinal absorption of drugs via solid solutions and eutectic mixtures III: experimental evaluation of griseofulvin-succinic acid solid solution*, J Pharm Sci 55 (1966) 487-492.
- [27] Goodman L.S., Gilman A., *The pharmacological bases of therapeutics*, 8th Ed, Pergamon Press, New York (1990).
- [28] Gordon M., Taylor J.S., *Ideal copolymers and the 2nd-order transitions of synthetic rubbers 1. Non-crystalline copolymers*, J Appl Chem 2 (1952) 493-500.
- [29] Grzybowska K., Capaccioli, S., Paluch, M., *Recent developments in the experimental investigations of relaxations in pharmaceuticals by dielectric techniques at ambient and elevated pressure*, Adv Drug Del Rev 100 (2016) 158-162.
- [30] Grzybowska K. et al., *Molecular dynamics and physical stability of amorphous anti-inflammatory drug: Celecoxib*, J Phys Chem B 114 (2010) 12792-12801.
- [31] Hancock B.C., Parks M., *What is the true solubility advantage for amorphous pharmaceuticals?*, Pharm Res 17 (2000) 397-404.
- [32] Hardung H., Djuric D., Ali S., *Combining HME & solubilization: Soluplus®-the solid solution*, Drug Delivery Tech 10 (2010) 20-27.

- [33] Havriliak S., Negami S., *A complex plane representation of dielectric and mechanical relaxation processes in some polymers*, Polymer 8 (1967) 161-210.
- [34] Jones R.A.L., *Soft condensed matter*, Oxford University Press, Oxford (2002).
- [35] Kauzmann W., *The nature of the glassy state and the behavior of liquids at low temperatures*, Chem Rev 43 (1948) 219-256.
- [36] Konno H. et al., *Effect of polymer type on dissolution profile of amorphous solid dispersion containing felodipine*, Eur J Pharm Biopharm (2008) 493-499.
- [37] Kothari K., Ragoonanan V., Suryanarayanan R., *The role of drug-polymer hydrogen bonding interactions on the molecular mobility and physical stability of nifedipine solid dispersions*, Mol Pharmaceutics 12 (2015) 162-170.
- [38] Kremer F., Schönhals A., *Broadband Dielectric Spectroscopy*, Springer-Verlag, Berlin Heidelberg (2003).
- [39] Kyeremateng, S.O., Pudlas, M., Woehrle, G.H., *A fast and reliable empirical approach for estimating solubility of crystalline drugs in polymers for hot melt extrusion formulations*, J Pharm Sci 103 (2014) 2847-2858.
- [40] Lan, Y., Ali, S., Langley, N., (2010) *Characterization of Soluplus by FTIR and Raman Spectroscopy*, CRS 2010 Annual Conference, At Portland, Oregon, U.S.A.
- [41] Lipinski C.A. et al., *Experimental and computational approaches to estimate solubility and permeability in drug discovery and development settings*, Adv Drug Delivery Rev 23 (1997) 3-25.
- [42] Marsac P.J., Konno H., Taylor L.S., *A comparison of the physical stability of amorphous felodipine and nifedipine systems*, Pharm Res 23 (2006) 2306-2316.
- [43] Massalska-Arods M. et al., *Molecular dynamics and crystallization behavior of chiral isooctylloxycyanobiphenyl as studied by dielectric spectroscopy*, J Phys Chem B 103 (1999) 4197-4205.
- [44] Mendiratta C., Kadam V., Pokharkar V., *Lansoprazole solid dispersion using a novel amphiphilic polymer Soluplus®*, J Chem Pharm Res 3 (2011) 536-543.

-
- [45] Mistry P. et al, *Role of the strength of drug-polymer interactions on the molecular mobility of crystallization inhibition in Ketoconazole solid dispersions*, Mol Pharmaceutics 12 (2015) 3339-3350.
- [46] Miyazaki T. et al., *Ability of polyvinylpyrrolidone and polyacrylic acid to inhibit the crystallization of amorphous acetaminophen*, J Pharm Sci 93 (2004) 2710-2717.
- [47] Muela S. et al., *Influence of temperature on the solubilization of thiabendazole by combined action of solid dispersion and co-solvents*, Int J Pharm 384 (2010) 93-99.
- [48] Napolitano S., Wübbenhorst M., *Monitoring the cold crystallization of poly(3-hydroxy butyrate) via dielectric spectroscopy*, J Non-Crystalline Solids 353 (2007) 4357-4361.
- [49] Nascimento M.L.F., Aparicio C., *Data classification with the Vogel-Fulcher-Tammann-Hesse viscosity equation using correspondence analysis* Physica B 398 (2007) 71-77.
- [50] Vueba, M.L., Pina, M.E., Batista de Carvalho, L.A.E., *Conformational stability of ibuprofen: assessed by DFT calculations and optical vibrational spectroscopy*, J Pharm Sci 97 (2008) 845-859.
- [51] O'Donnell K.P., Woodward W.H., *Dielectric spectroscopy for the determination of the glass transition temperature of pharmaceutical solid dispersions*, Informa Healthcare (2014) 1-14.
- [52] Paradkar A. et al., *Characterization of curcumin-PVP solid dispersion obtained by spray drying*, Int J Pharm 271 (2004) 281-286.
- [53] Paudel A., Van Humbeeck J., Van den Mooter G. *Theoretical and experimental investigation on the solid solubility and miscibility of naproxen in poly(vinylpyrrolidone)*, Mol Pharm 7 (2010) 1133-1148.
- [54] Qian F. et al, *Is a distinctive single Tg a reliable indicator for the homogeneity of amorphous solid dispersion?*, Int J of Pharm 395 (2010) 232-235.

- [55] Sekiguchi K., Obi N., *Studies on Absorption of Eutectic Mixture. I. A comparison of the behaviour of eutectic mixture of Sulfathiazole and that of ordinary Sulfathiazole in man*, Chemical and Pharmaceutical Bulletin 9 (1961) 866-872.
- [56] Sethia S., Squillante E., *Solid dispersion of carbamazepine in PVP K30 by conventional solvent evaporation and supercritical methods*, Int J Pharm 272 (2004) 1-10.
- [57] Singh, A. et al., *Effect of compression on the molecular arrangement of itraconazole-soluplus solid dispersions: induction of liquid crystals or exacerbation of phase separation?*, Mol Pharm Online, DOI: 10.1021/acs.molpharmaceut.6b00046.
- [58] Tammann G., *Glasses as supercooled liquids*, J Soc Glass Tech 9 (1925) 166-1850.
- [59] Taylor L.S., Zografi G., *Spectroscopic characterization of interactions between PVP and indomethacin in amorphous molecular dispersions*, Pharm Res 14 (1997), 1691-1698.
- [60] Thomas L.C., *Modulated DSC Paper #3 Modulated DSC Basics; Optimization of MDSC Experimental Conditions*, Retrieved at <http://www.tainstruments.com>, 2016-01-27.
- [61] Thomas L.C., *Modulated DSC Paper #1 Why Modulated DSC? ; An Overview and Summary of Advantages and Disadvantages Relative to Traditional DSC*, Retrieved at http://www.tainstruments.com/main.aspx?n=2&id=181&main_id=891&siteid=11, 2016-01-27.
- [62] Tian Y. et al., *Construction of drug-polymer thermodynamic phase diagram using Flory-Huggins interaction theory: identifying the relevance of temperature and drug weight fraction to phase separation within solid dispersions*, Mol Pharm 10 (2013) 236-248.
- [63] Van der Mooter G. et al., *Physical stabilization of amorphous ketoconazole in solid dispersions with polyvinylpyrrolidone K25*, Eur J Pharm Sci 12 (2001) 261-269.

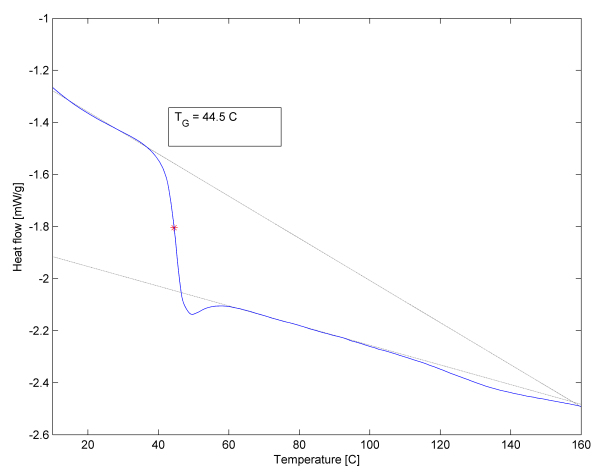
- [64] Van Drooge D.J. et al., *Characterization of the molecular distribution of drugs in glassy solid dispersions at the nano-meter scale, using differential scanning calorimetry and gravimetric water vapour sorption techniques*, Int J Pharm 310 (2006) 220–229.
- [65] Van Drooge D.J. et al., *Anomalous dissolution behavior of tablets prepared from sugar glass-based solid dispersions*, J Controlled Release 97 (2004) 441–452.
- [66] Williams H.D. et al., *Strategies to address low drug solubility in discovery and development* Pharmacological Rev (2013) 315-499.
- [67] Won D-H. et al., *Improved physicochemical characteristics of felodipine solid dispersion particles by supercritical anti-solvent precipitation process*, Int J Pharm 301 (2005) 199-208.
- [68] Zhou, D. et al., *Physical stability of amorphous pharmaceuticals: importance of configurational thermodynamic quantities and molecular mobility*, J Pharm Sci 91 (2002) 1863-1872.

A

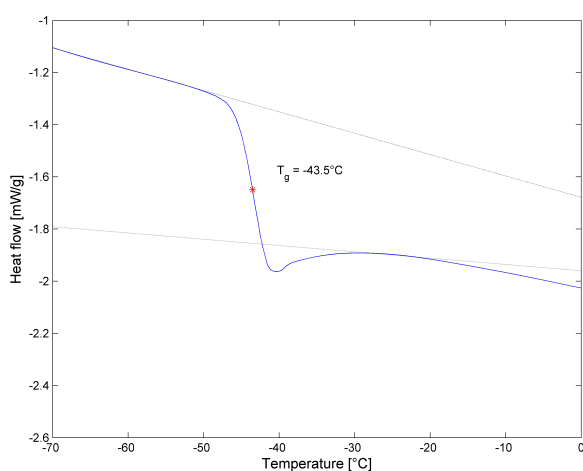
Supporting Information

A.1 DSC thermograms

Figure A.1-A.3 present the thermograms for all neat components. Several measurements were made to confirm results.

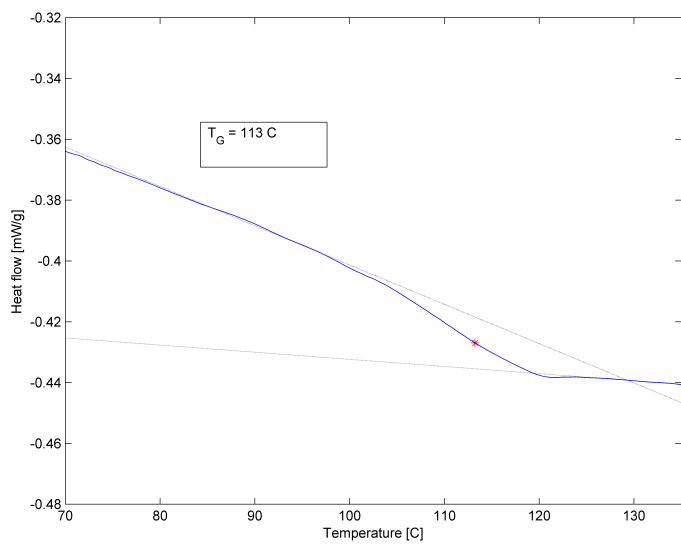


(a)

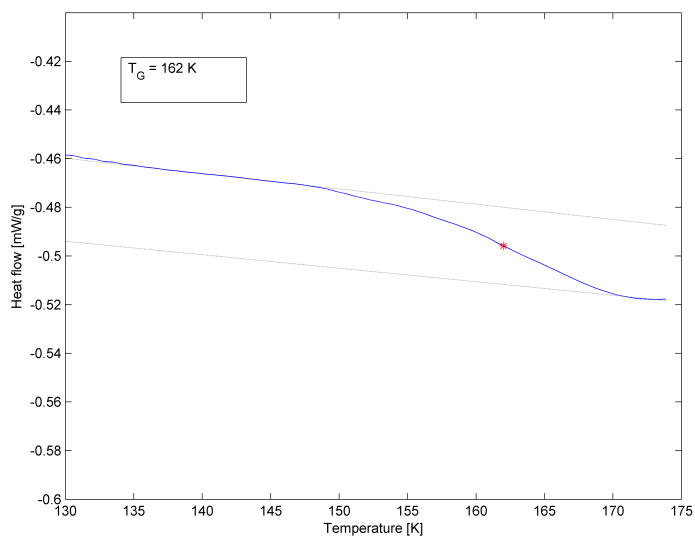


(b)

Figure A.1: a) *Felodipine powder.* b) *Ibuprofen powder.*



(a)



(b)

Figure A.2: a) Solvent casted HPMCAS film. b) PVP K30 powder.

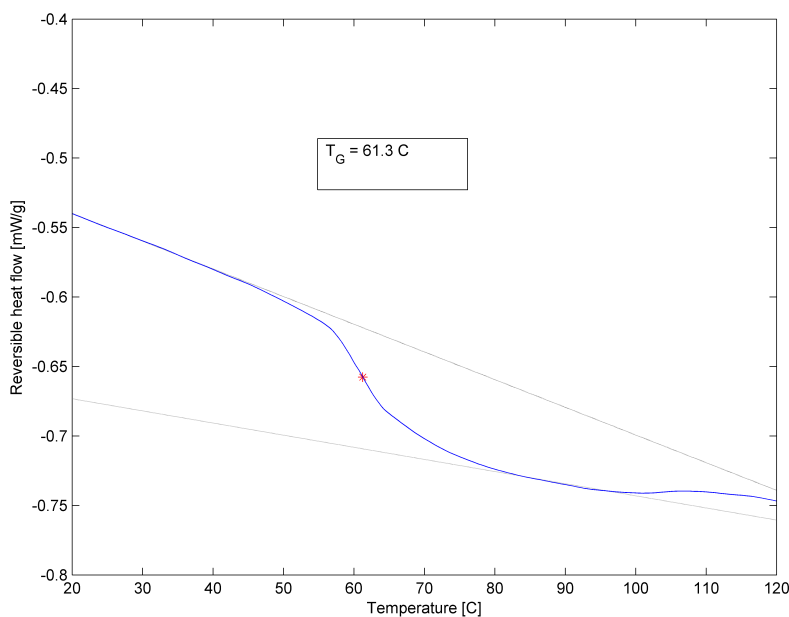


Figure A.3: *Soluplus* powder.

A.2 Raman Analysis

To investigate the differences shown in the DSC measurements of PVP:IP20 dispersions in the top left figure in figure A.4, Raman Spectroscopy was utilized. Raman spectroscopy studies the vibrational and rotational modes of the sample by using a monochromatic light source to illuminate the sample and then analyzing the scattered light. Using this method it is possible to spot traces of solvent left in the dispersion, which was the hypothesis for the shifted T_g of the dispersions. Firstly, all neat substances were analyzed to have reference spectra and then the dispersions spectra were compared to these. A Bruker MultiRAM Stand Alone FT-Raman Spectrometer was used. The spectral range was $3600 - 50 \text{ cm}^{-1}$ (Stokes shift), and a wavelength of 1064 nm and intensity of 400 mW was used for the laser. All samples were scanned 1000 times to increase signal resolution.

From figure A.4 c) and d) it can be seen that the difference between the dispersions in a) is most likely to come from a difference in PVP concentration. The spectrum from the solvent mixture does not appear clearly in the dispersion spectra and therefore it is possible to rule out the solvent impact. The increased PVP content in the dispersion prepared 1102 also explains the elevated glass transition temperature shown in a).

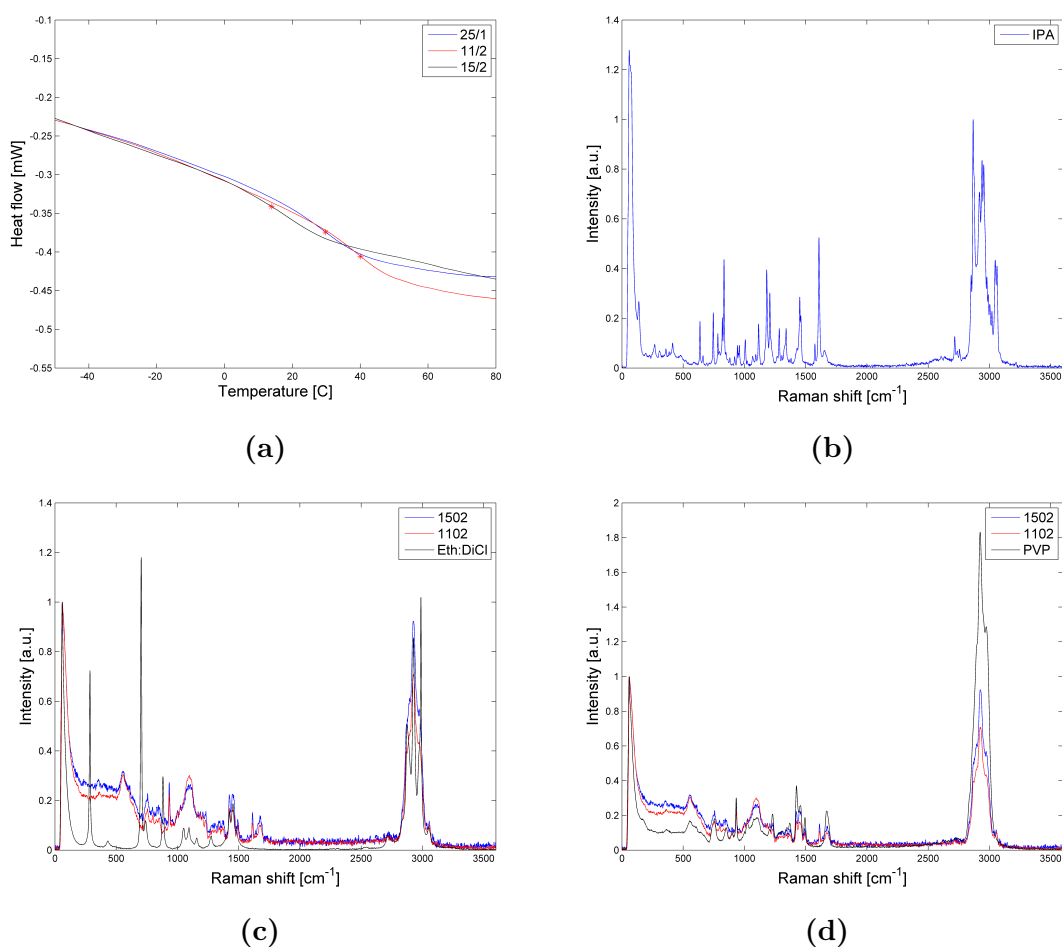


Figure A.4: a) DSC thermograms of PVP:IP20 dispersions prepared on three different dates. b) Raman spectrum of amorphous ibuprofen. c) Raman spectrum of two different dispersions and the solvent mixture. d) Raman spectrum of two different dispersions and pure PVP.

A.3 Crystallization Kinetics

The following section presents data from crystallization monitoring using dielectric spectroscopy.

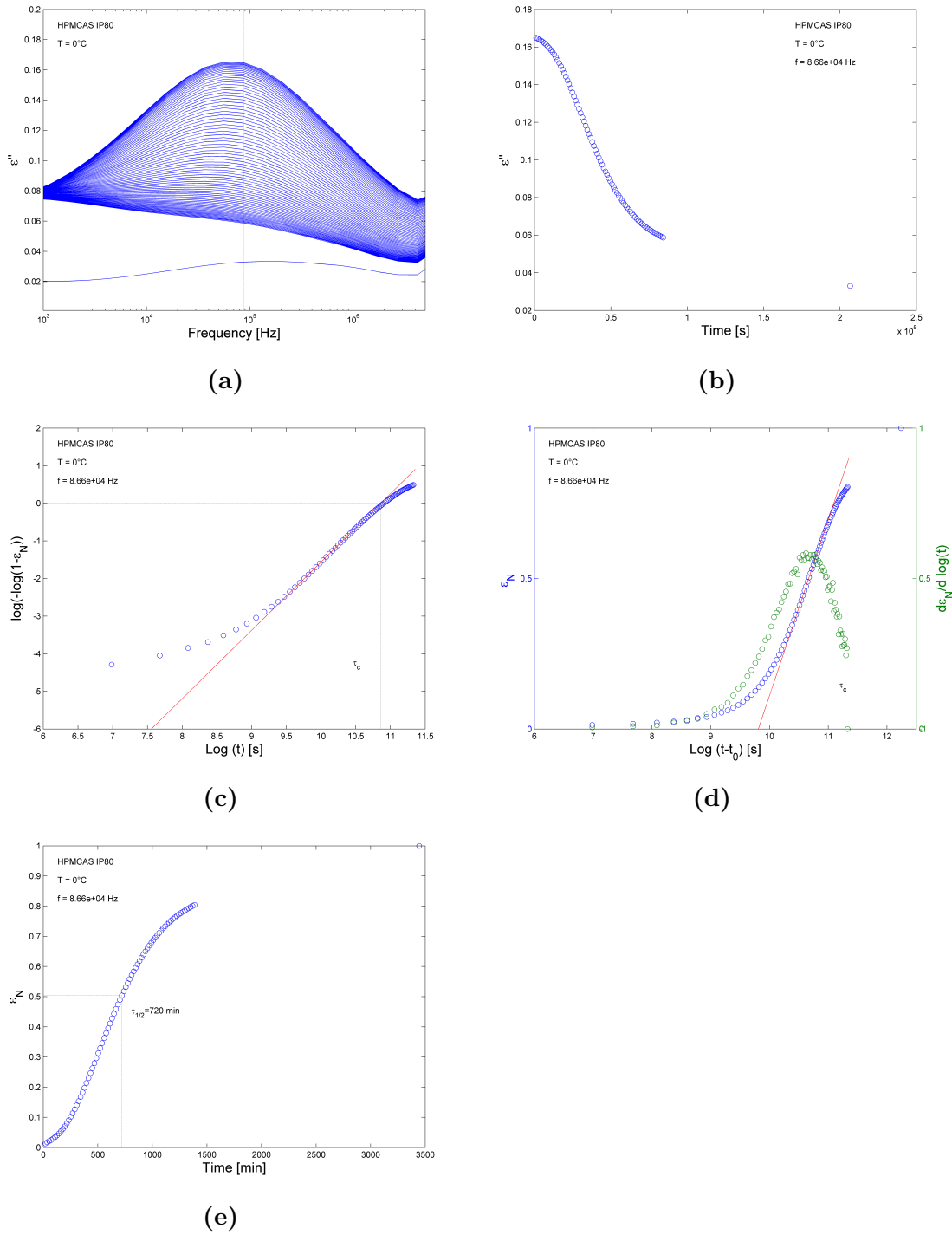


Figure A.5: a) Dielectric spectrum of HPMCAS:IP80 at 0 °C monitored for 24 h together with a measurement after 50 h using protocol i. The analyzed frequency ($8.7e4$ Hz) is marked with the vertical line. b) Strength of the dielectric signal at $8.7e4$ Hz vs time. c) Avrami plot. d) Avramov plot marking the crystallization timescale τ_c . e) Normalized dielectric signal vs time where the halfpoint crystallization time $\tau_{1/2}$ is marked.

A. Supporting Information

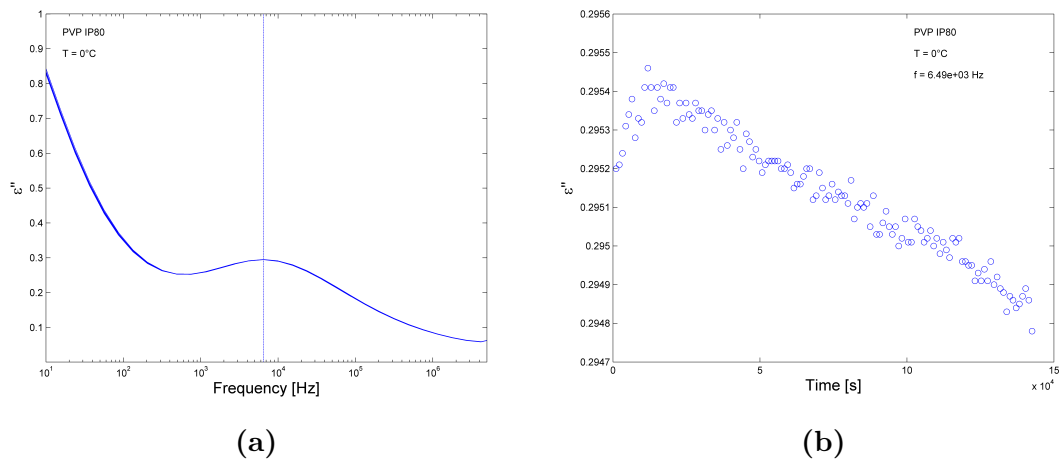


Figure A.6: *a)* Dielectric spectrum of PVP:IP80 at 0°C monitored for 40 h using protocol *i*. The analyzed frequency (6.5×10^3 Hz) is marked with the vertical line. No decrease in the signal can be seen. *b)* Strength of the dielectric signal at 6.5×10^3 Hz vs time. The decrease in signal strength is $< 1\%$, thus confirming fully inhibited crystallization.

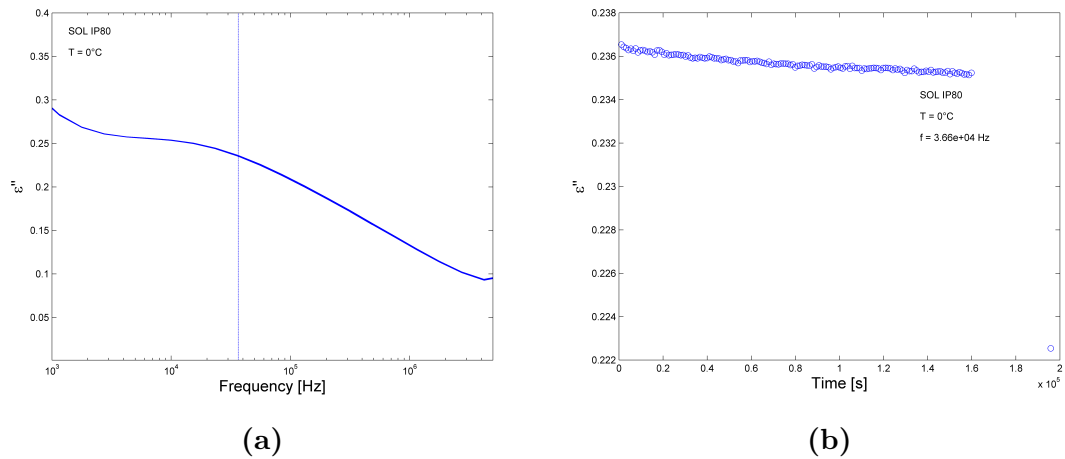


Figure A.7: *a)* Dielectric spectrum of SOL:IP80 at 0°C monitored for 55 h using protocol *i*. The analyzed frequency (3.66×10^4 Hz) is marked with the vertical line. A very small decrease in the signal can be seen. *b)* Strength of the dielectric signal at 3.66×10^4 Hz vs time. The decrease in signal strength of the last measurement point is around 5%, thus suggesting a start of the crystallization process.

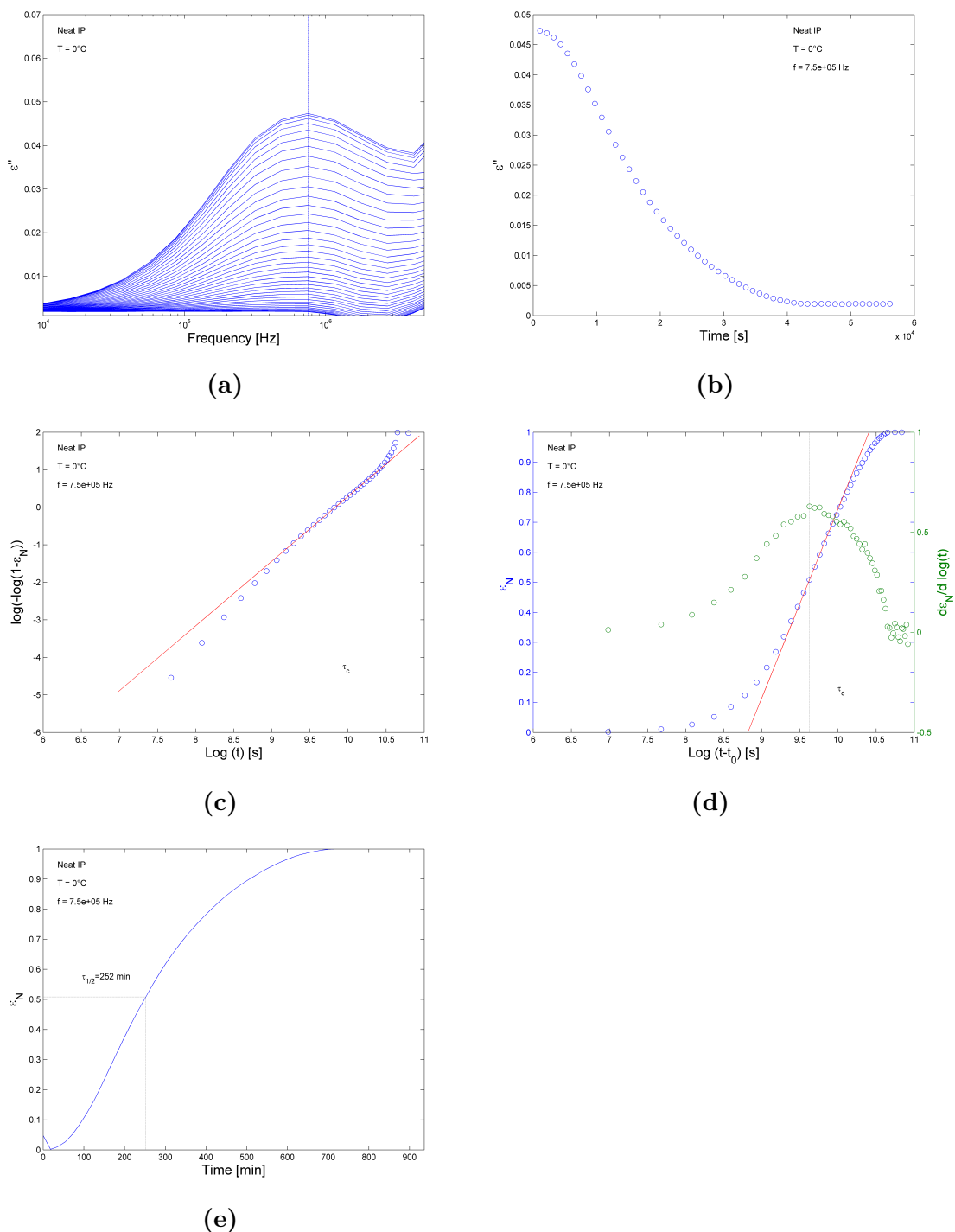


Figure A.8: a) Dielectric spectrum of ibuprofen at 0 °C monitored for 24 h using protocol ii, the analyzed frequency (7.5e5 Hz) is marked with the vertical line. b) Strength of the dielectric signal at 7.5e5 Hz vs time. c) Avrami plot. d) Avrami plot marking the crystallization timescale τ_c . e) The normalized dielectric signal vs time where the halfpoint crystallization time $\tau_{1/2}$ is marked.

A. Supporting Information

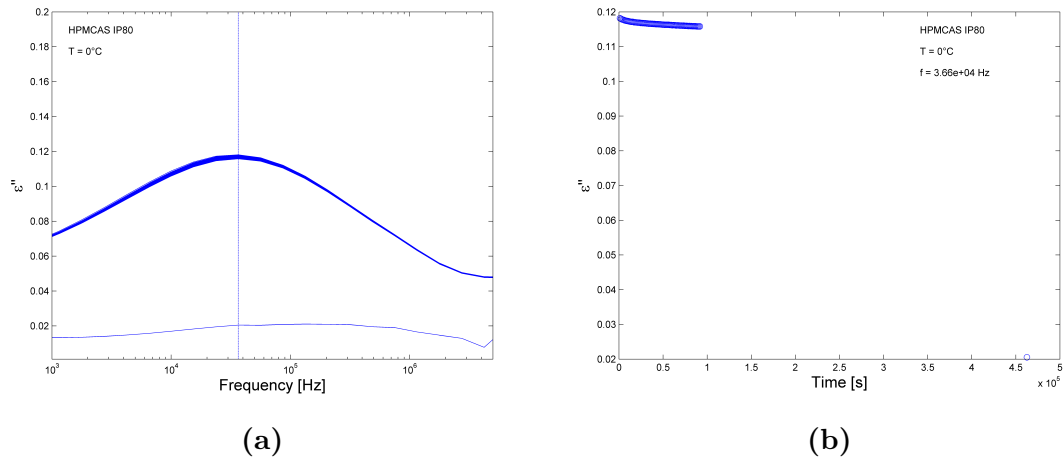


Figure A.9: a) Dielectric spectrum of HPMCAS:IP80 at 0 °C monitored for 40 h using protocol ii and a subsequent measurement after 165 h. The analyzed frequency (3.66×10^4 Hz) is marked with the vertical line. A very small decrease in the signal can be seen. b) Strength of the dielectric signal at 3.66×10^4 Hz vs time. Full crystallization can be seen after 125 h, but no significant crystallization is seen up to 40 h.

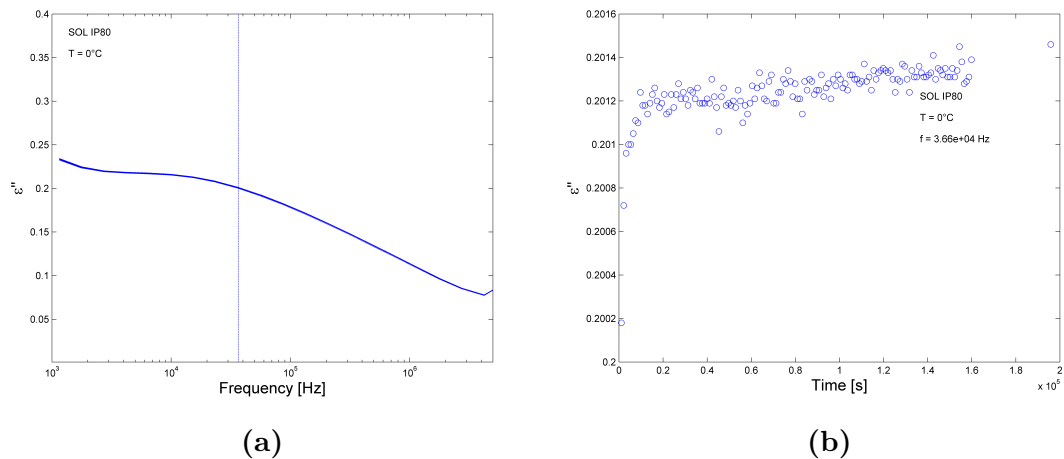


Figure A.10: a) Dielectric spectrum of SOL:IP80 at 0 °C monitored for 44 h using protocol ii and a subsequent measurement after 55 h. The analyzed frequency (3.66×10^4 Hz) is marked with the vertical line. b) Strength of the dielectric signal at 3.66×10^4 Hz vs time. No decrease in dielectric strength can be seen, but rather a tiny increase.

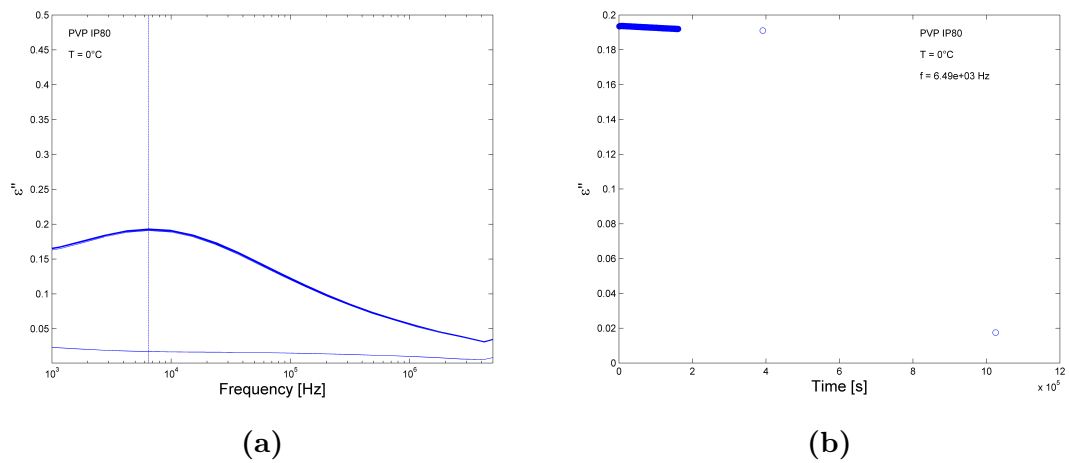


Figure A.11: a) Dielectric spectrum of PVP:IP80 at 0 °C monitored for 44 h using protocol ii and a subsequent measurement after 245 h. The analyzed frequency (6489 Hz) is marked with the vertical line. b) Strength of the dielectric signal at 6489 Hz vs time. What is thought to be full crystallization can be seen after 245 h.